Modelling and Design of Millimeter-Wave Networks for Highway Vehicular Communication

Andrea Tassi, Malcolm Egan, Robert J. Piechocki and Andrew Nix

***Abstract*—Connected and autonomous vehicles will play a pivotal role in future Intelligent Transportation Systems (ITSs) and smart cities, in general. High-speed and low-latency wireless communication links will allow municipalities to warn vehicles against safety hazards, as well as support cloud-driving solutions to drastically reduce traffic jams and air pollution. To achieve these goals, vehicles need to be equipped with a wide range of sensors generating and exchanging high rate row-data streams. Recently, millimeter wave (mmWave) techniques have been introduced as a means of fulfilling such high data rate requirements. In this paper, we model a highway communication network and characterize its fundamental link budget metrics. In particular, we specifically consider a network where vehicles are served by mmWave Base Stations (BSs) deployed alongside the road. To evaluate our highway network, we develop a new theoretical model that accounts for a typical scenario where heavy vehicles (such as buses and lorries) in slow lanes obstruct Line-of-Sight (LOS) paths of vehicles in fast lanes and, hence, act as blockages. Using tools from stochastic geometry, we derive approximations for the Signal-to-Interference-plus-Noise ratio (SINR) outage probability, as well as the probability that a user achieves a target communication rate (rate coverage probability). Our analysis provides new design insights for mmWave highway communication networks. In particular, we show that smaller antenna beamwidths and, unlike bi-dimensional mmWave cellular networks, smaller BS densities do not necessarily have a disruptive impact on improving the SINR outage probability, and consequently the rate coverage probability.**

***Index Terms*—Vehicular communications, millimeter-wave networks, performance modelling, stochastic geometry.**

I. Introduction

By 2020, fifty billion devices will have connectivity capabilities [1]. Among these, ten million vehicles equipped with on-board communication systems and with a variety of autonomous capabilities will be progressively rolled out. According to the National Highway Traffic Safety Administration (U.S. Department of Transportation) and the European Commission's Connected-Intelligent Transportation System (C-ITS) initiative [2], [3], connectivity will allow vehicles to engage with future ITS services, such as See-Through, Automated Overtake, High Density Platooning, etc [4].

As identified by the European Commission's C-ITS initiative, the number of sensors mounted on each vehicle has increased. A typical sensor setup is expected to range from ultrasound proximity sensors to more sophisticated camcorders and 'Light Detection And Ranging' (LiDAR) systems [4]. Currently, the number of on-board sensors are around 100 units and this number is expected to double by 2020 [5]. Ideally, the higher the number of on-board sensors, the "smarter" the vehicle. However, this holds true only if vehicles are able to exchange the locally sensed data [6]. For instance, multiple LiDAR-equipped vehicles may approach a road hazard and share their real-time LiDAR data with incoming vehicles by means of the road-side infrastructure. This allows the approaching vehicles to compensate for their lack of sensor data (blind-spot removal) and, for instance, help smart cruise-control systems make decisions. As such, there are strong constraints on LiDAR data delivery, which can be generated at rates up to $100\,\mathrm{Mbps}$. More generally, semi-autonomous and full-autonomous vehicles will require high rate and low latency communication links to support the applications envisaged by the 5G Infrastructure Public Private Partnership's (5G-PPP). These applications include the See-Through use case (maximum latency equal to $50\,\mathrm{ms}$), which enables vehicles to share live video feeds of their onboard cameras to following vehicles. Other applications such as Automated Overtake and High Density Platooning are also expected to require communication latencies smaller than $10\,\mathrm{ms}$ [4, Table 1].

Recently, communication systems operating in the millimeter-wave (mmWave) range of the wireless spectrum have been proposed as a means of overcoming the rate and latency limitations of existing technologies [7], [8]. In fact, currently commercialized mmWave systems can already ensure up to $7\,\mathrm{Gbps}$ and latencies smaller than $10\,\mathrm{ms}$ [9]. Table I summarizes the general performance metrics of mmWave systems and compares them with the main technologies adopted to enable infrastructure-to-vehicle communications. Traditionally, ITSs rely on Dedicated Short-Range Communication (DSRC) standards, such as IEEE 802.11p/DSRC and ITS-G5/DSRC [10]–[13]. Even though these technologies operate in a licensed band and ensure low communication latencies, their maximum realistic data rate hardly exceeds $6\,\mathrm{Mbps}$ [10]. As such, several papers [14], [15] suggest the adoption of 3GPP's Long Term Evolution-Advanced (LTE-A), which can guarantees higher communication rates. Nevertheless, the maximum supported data rate is limited to $100\,\mathrm{Mbps}$ and end-to-end latencies cannot go below $100\,\mathrm{ms}$ [6]. As a result, both DSRC and LTE-A cannot meet the communication constraints dictated by future ITS applications [4, Table 1].

In mmWave systems, both Base Stations (BSs) and users are equipped with large antenna arrays to achieve high array gains via beamforming techniques [16]. As mmWave systems

A. Tassi, R. J. Piechocki and A. Nix are with the Department of Electrical and Electronic Engineering, University of Bristol, UK (e-mail: {a.tassi,r.j.piechocki,Andy.Nix}@bristol.ac.uk).

M. Egan is with the CITI Laboratory of the Institut National de Recherche en Informatique et en Automatique (INRIA), Université de Lyon, and Institut National de Sciences Apliquées (INSA) de Lyon, FR (e-mail: malcom.egan@inria.fr).

TABLE I
RADIO ACCESS SOLUTIONS FOR VEHICULAR COMMUNICATIONS.

	IEEE 802.11p/DSRC, ITS-G5/DSRC [13]	**LTE-A** [15]	**mmWave Systems** [9]
Frequency Band	5.85 GHz - 5.925 GHz	Spanning multiple bands in 450 MHz - 4.99 GHz	28 GHz, 38 GHz, 60 GHz bands and E-band
Channel Bandwidth	10 MHz	Up to 100 MHz	100 MHz-2.16 GHz
Bit Rate	3 Mbps-27 Mbps	Up to 1 Gbps	Up to 7 Gbps
Latency	≤ 10 ms	100 ms-200 ms	≤ 10 ms
Mobility Support	$\leq 130\,\mathrm{km\,h^{-1}}$	$\leq 350\,\mathrm{km\,h^{-1}}$	$\leq 100\,\mathrm{km\,h^{-1}}$
MIMO	Not supported	$\leq 8 \times 8$ in downlink and $\leq 4 \times 4$ in uplink	$\geq 10 \times 10$

operate in the portion of the spectrum between 30 GHz and 300 GHz [9], mmWave links are highly sensitive to blockages. In particular, line-of-sight (LOS) communications are characterized by path loss exponents that tend to be smaller than 2.8, while non-line-of-sight (NLOS) path loss exponents are at least equal to 3.8 [17]. Due to of the high NLOS path loss and the difficulty of beam alignment, commercial mmWave solutions cannot support user speeds greater than $100\,\mathrm{km\,h^{-1}}$. Despite this, research to cope with mobile users is gaining momentum [18]. For instance, in the UK, the main railways stakeholders are already trialling mmWave systems with enhanced beam searching techniques to provide broadband wireless connectivity onboard moving trains [19]. In addition, multiple research initiatives already regard mmWave systems as suitable to deploy 5G dense cellular networks [20]–[22].

In this paper, we consider a typical road-side infrastructure for ITSs [23]. In particular, the infrastructure-to-vehicle communications required by ITS services are handled by a dedicated network of BSs placed at the sides of the road usually fitted at the top of lampposts and other roadside locations, typically on both sides of the road [24], [25]. We deal with a highway system where vehicles receive high data rate streams transmitted by mmWave BSs, although we do not consider scenarios where there is no roadside deployment of BSs where vehicle-to-vehicle communication technologies may provide a more effective solution. A key feature of our highway system is that vehicles with different sizes are likely to drive along the same set of lanes. In a left-hand traffic system, any slow vehicle (such as double decker buses or lorries) typically travels in the outermost lanes of the highway, while the other vehicles tend to drive along the innermost lanes. As a consequence, if a larger vehicle drives between a user and its serving BS, the BS is no longer in LOS. In other words, large vehicles may act as communication blockages.

We develop a new framework to analyze and design mmWave communication systems. The original contributions of this paper are summarized as follows:

- We propose the first theoretical model to characterize the link budget requirements of mmWave networks providing downlink connectivity to highway vehicles where communications are impaired by large vehicles acting as communication blockages. Specifically, we offer design insights that take into account how the BS and blockage densities impact the user achievable data rate.
- We show that the performance of mmWave highway networks can be well approximated by our theoretical model, which assumes that both BS and blockage positions are governed by multiple time-independent mono-dimensional PPPs. This makes the proposed model tractable and allows us to predict user performance in scenarios characterized by different BS densities, traffic intensities, antenna gain and directivity.
- Our numerical validation demonstrates that the proposed theoretical model captures key features of the system. In particular, we observe that a smaller antenna beamwidth does not necessarily reduce the Signal-to-Interference-plus-Noise Ratio (SINR) outage probability. Furthermore, we show that the SINR outage probability in highway mmWave networks is minimized by low density BS deployments, for a fixed probability threshold.

The reminder of the paper is organized as follows. Section II discusses the related work on mmWave and vehicular communication systems. Section III presents our mmWave communication system providing downlink coverage in highway mmWave networks. We evaluate the network performance in terms of the SINR outage and rate coverage probabilities, which are derived in Section IV. Section V validates our theoretical model. In Section VI, we conclude and outline avenues of future research.

II. RELATED WORK

As summarized in Table II, over the past few years, mmWave systems have been proposed as a viable alternative to traditional wireless local area networks [26] or as a wireless backhauling technology for BSs of the same cellular network [27], [28]. Furthermore, mmWave technology has also been considered for deploying dense cellular networks characterized by high data rates [21], [30], [31]. With regards to the vehicular communication domain, J. Choi *et al.* [7] pioneered the application of the mmWave technology to partially or completely enable ITS communications. A mmWave approach to ITS communications is also being supported by the European Commission, which recently identified the possibility of designing ITSs that rely on technologies operating in the band spanning 63–64 GHz [3].

As both the BS deployment and vehicle locations differ over both time and in different highway regions, any highway network model must account for these variations. In this setting, stochastic geometry provides a means of characterizing the performance of the system by modelling BS locations via a spatial process, such as the Poisson Point Process (PPP) [36]. Generally, PPP models for wireless networks are now a well established methodology [8], [36]–[40]; however there are challenges in translating standard results into the context of mmWave networks for road-side deployments due to the presence of NLOS links resulting from blockages [21]. In particular, the presence of blockages has only been addressed

TABLE II
RELATED WORKS ON MMWAVE SYSTEMS AND VEHICULAR COMMUNICATIONS.

Ref.	Radio Access Technology	Network Topology	Channel and Path Loss Models	Mobility	Communication Blockages
[7]	mmWave	Vehicle-to-vehicle, Vehicle-to-infrastructure	Based on ray-tracing	Vehicles moving on urban roads	Not analytically investigated
[21]	mmWave	Dense cellular network	Nakagami small-scale fading; BGG path loss model	Static blockages	Buildings
[26]	mmWave	Dense cellular system	Based on measurements	Static blockages	Buildings
[27]	mmWave	Network backhauling	Constant small-scale fading (i.e., the square norm of the small-scale fading contribution is equal to 1)	Static blockages	None
[28]	mmWave	Cellular network with self-backhauling	Constant small-scale fading; BGG path loss model	Static blockages	Buildings
[29]	mmWave	Co-operative cellular network	Nakagami for the signal, Rayleigh for the interference contribution; BGG path loss model	Static blockages	Buildings
[30]	mmWave	Cellular network with self-backhauling	Based on measurements	Static blockages	Indoor objects
[31]	mmWave	Multi-tier cellular network	Constant small-scale fading; Probabilistic path loss model	Static blockages	Buildings
[32]	DSRC	Vehicle-to-vehicle, Vehicle-to-infrastructure	Coverage-based (i.e., no packet errors from nodes within the radio range)	Vehicles moving on urban roads	None
[33]	DSRC	Vehicle-to-vehicle, Vehicle-to-infrastructure	Rice small-scale fading	Vehicles moving on urban roads	None
[34]	DSRC	Vehicle-to-vehicle	Obstacle-based channel and path loss models	Vehicles moving on a highway	Vehicles
[35]	DSRC	Vehicle-to-vehicle	Rayleigh small-scale fading	Vehicles moving on a highway	None

in the context of mmWave cellular networks in urban and suburban environments that that are substantially different to a highway deployment [21]. In particular, in mmWave cellular networks: (i) the positions of BSs follow a bi-dimensional PPP, and (ii) the positions of blockages are governed by a stationary and isotropic process. Even though this is a commonly accepted assumption for bi-dimensional cellular networks [36], this is not satisfied by highway scenarios, where both blockages and BS distributions are clearly not invariant to rotations or translations. With regards to Table II, the path loss contribution of blockages has either been modeled by means of the Boolean Germ Grain (BGG) principle (i.e., only the BSs within a target distance are in LOS) or in a probabilistic fashion (i.e., a BS is in LOS/NLOS with a given probability). To the best of our knowledge, no models for road-side mmWave BS deployment accounting for vehicular blockages have been proposed to date.

Given the simplicity of their topology and their high level of automation, highway scenarios have been well investigated in the literature [32]–[34]. In particular, [32] addresses the issue of optimizing the density of fixed transmitting nodes placed at the side of the road, with the objective of maximizing the stability of reactive routing strategies for Vehicular Ad-Hoc Networks (VANETs) based on the IEEE 802.11p/DSRC stack. Similar performance investigations are conducted in [33] where a performance framework jointly combining physical and Media Access Control (MAC) layer quality metrics is devised. In contrast to [32] and [33], [34] addresses the issue of blockage-effects caused by large surrounding vehicles; once more, [34] strictly deals with IEEE 802.11p/DSRC communication systems. The proposal in [32]–[34] is not applicable for mmWave highway networks as the propagation conditions of a mmWave communication system are not comparable with those characterizing a system operating between $5.855\,\mathrm{GHz}$ and $5.925\,\mathrm{GHz}$. Another fundamental difference with between mmWave and IEEE 802.11p/DSRC networks is the lack of support for antenna arrays capable of beamforming as the IEEE 802.11p/DSRC stack is restricted to omnidirectional or non-steering sectorial antennas.

Highway networks have also been studied using stochastic geometry. In particular, M. J. Farooq *et al.* [35] propose a model for highway vehicular communications that relies on the physical and MAC layers of an IEEE 802.11p/DSRC or ITS-G5/DSRC system. As such, the access to the medium is regulated by the Carrier Sense Multiple Access (CSMA) protocol. In addition, antennas are strictly omnidirectional and all transmissions occur in LOS. The key differences between this paper and [35] are: (i) [35] focuses on multi-hop inter-vehicle communications and routing strategies while our paper deals with one-hop infrastructure-to-vehicle coverage issues, (ii) [35] considers communication devices with no beamforming capabilities while beamforming is a key aspect of our mmWave system, and (iii) [35] does not consider the possibility of having NLOS communications, which is a substantial part of our analysis.

III. SYSTEM MODEL AND PROPOSED BS-STANDARD USER ASSOCIATION SCHEME

We consider a system model where mmWave BSs provide network coverage over a section of a highway, illustrated in Fig. 1. The goal of our performance model is to characterize the coverage probability of a user surrounded by several moving blockages (i.e., other vehicles) that may prevent a target user to be in LOS with the serving BS. Without loss of generality, we consider the scenario where vehicles drive

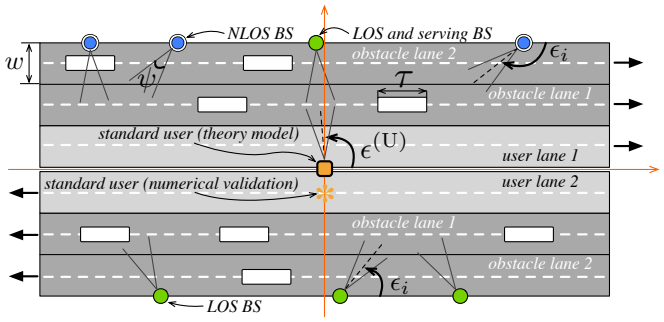

Fig. 1. Considered highway system model, composed of $N_o = 2$ obstacle lanes in each traffic direction.

on the left hand side of the road[1]. For clarity, Table III summarizes the symbols commonly used in the paper. In order to gain insight into the behavior of the model, we make the following set of assumptions.

Assumption 3.1 (Road Layout): We assume that the whole road section is constrained within two infinitely long parallel lines, the *upper* and *bottom sides* of the considered road section. Vehicles flow along multiple parallel lanes in only two possible directions: West-to-East (for the upper-most lanes) and East-to-West (for the lowermost lanes). Each lane has the same width w. For each direction, there are N_o obstacle lanes and one user lane closer to the innermost part of the road. The closer a lane is to the horizontal symmetry axis of the road section, the more the average speed is likely to increase – thus, the large/tall vehicles are assumed to drive along obstacle lanes most of the time. Vehicles move along the horizontal symmetry axis of each lane. We use a coordinate system centered on a point on the line separating the directions of traffic. The upper side of the road intercepts the y-axis of our system of coordinates at the point $(0, w(N_o+1))$, while the bottom side intercepts at $(0, -w(N_o+1))$.

In the following sections, we will focus on characterizing the performance of the downlink phase of a mmWave cellular network providing connectivity to the vehicles flowing in the high speed lanes of the considered model, which is challenging. In fact, communication links targeting users in the high speed lanes are impacted by the largest number of communication blockages (namely, large vehicles) flowing on on the outer road lanes.

Since mmWave technologies for ITS applications are a relatively new research topic, to the best of our knowledge we are not aware of any large-scale urban or highway cellular deployment currently running with this technology. As such, our analysis cannot directly refer to any existing mmWave network. Moreover, there is a need for basic design strategies for large-scale highway mmWave networks. To this end, we adopt the standard assumption of the BSs being distributed according to a PPP, which is typical in stochastic geometry.

Assumption 3.2 (BS Distribution): Let $\Phi_{\mathrm{BS}} = \{x_i\}_{i=1}^{b}$ be the one-dimensional PPP, with density λ_{BS} of the x-components of the BS locations on the road. We assume that BSs are located along with the upper and bottom sides of the road section. In particular, the i-th BS lies on the upper or bottom sides with a probability equal to $q = 0.5$. In other words, the y-axis coordinate of the i-th BS is defined as $y_i = w(-2\mathbb{B}_q+1)(N_o+1)$, where $\mathbb{B}_q$ is a Bernoulli random variable with parameter q.

By Assumption 3.2 and from the independent thinning theorem of PPP [41, Theorem 2.36], it follows that the x-axis coordinates of the BSs at the upper and bottom sides of the road form two independent PPPs with density $0.5 \cdot \lambda_{\mathrm{BS}}$.

Assumption 3.3 (Blockage Distribution): We assume that the ℓ-th obstacle lane on a traffic direction and the coordinates $(x_{\ell,i}^{(\mathrm{o})}, y_{\ell,i}^{(\mathrm{o})})$ of blockage i, $x_{\ell,i}^{(\mathrm{o})}$ belongs to a one-dimensional PPP $\Phi_{\mathrm{O},\ell}$ with density $\lambda_{\mathrm{o},\ell}$, for $\ell \in \{1, \ldots, N_o\}$ [35]. The term $y_{\ell,i}^{(\mathrm{o})}$ is equal to $w\ell$, or $-w\ell$, depending on whether we refer to the West-to-East or East-to-West direction, respectively. We assume that the density of the blockages of lane ℓ in each traffic direction is the same. Each blockage point is associated with a segment of length τ, centered on the position of the blockage itself and placed onto the horizontal symmetry axis of the lane (hereafter referred to as the "footprint segment"). Obstacles can be partially overlapped and the blockage widths and heights are not part of our modelling. The presence of large vehicles in the user lanes is regarded as sporadic and their impact on the user performance negligible – thus it is ignored.

From Assumption 3.3, given a driving direction, we observe that the blockage density of each obstacle lane can be different. This means that our model has the flexibility to cope with different traffic levels per obstacle lane; namely, the larger the traffic density, the larger the traffic intensity.

[1]Both the considered system model and the proposed theoretical framework can be easily extended to road systems where drivers are required to drive on the right hand side of the road.

TABLE III
COMMONLY USED NOTATION.

N_o	Number of obstacle lanes per driving direction
w	Width of a road lane
λ_{BS}	Density of the PPP Φ_{BS} of x-components of the BS locations on the road
$\lambda_{O,\ell}$	Density of the PPP $\Phi_{\mathrm{O},\ell}$ of x-components of the blockages on the ℓ-th obstacle lane
τ	Footprint segment of each blockage
p_{L}, p_{N}	Approximated probabilities of a BS being in LOS or NLOS with respect to the standard user, respectively
λ_{L}, λ_{N}	Densities of the PPPs of the x-components of LOS and NLOS BSs, respectively
$\ell(r_i)$	Path loss component associated with the i-th BS
A_{L}	Assuming the standard user connects to a NLOS BS at a distance r, it follows that there are no LOS BSs at a distance less or equal to $A_{\mathrm{L}}(r)$
A_{N}	Assuming the standard user connects to a LOS BS at a distance r, it follows that there are no NLOS BSs at a distance less or equal to $A_{\mathrm{N}}(r)$
$\mathrm{P_L}$, $\mathrm{P_N}$	Probabilities that the standard user connects to a LOS or a NLOS BS, respectively
G_{TX}, G_{RX}	Maximum transmit and receive antenna gains, respectively
g_{TX}, g_{RX}	Minimum transmit and receive antenna gains, respectively
$\mathcal{L}_{\mathrm{I_{S,E},\mathbb{E}_1}}(s)$	Laplace transform of the interference component determined by BSs placed on the upper (S = U) or bottom side (S = B) of the road that are in LOS (E = L) or in NLOS (E = N) to the standard user, conditioned on the serving BS being in LOS ($\mathbb{E}_1$ = L) or NLOS ($\mathbb{E}_1$ = N)
$\mathcal{L}_{\mathrm{I},\mathbb{E}_1}(s)$	Laplace transform of the interference I, given that the standard user connects to a LOS BS ($\mathbb{E}_1$ = L) or NLOS BS ($\mathbb{E}_1$ = N)
$\mathrm{P_T}(\theta)$	SINR outage probability as a function of SINR threshold θ
$\mathrm{R_C}(\kappa)$	Rate coverage probability as a function of target rate κ

Our primary goal consists of characterizing the SINR outage and rate coverage probability of users located on the user lanes, as these are the most challenging to serve due to the fact that vehicles in the other lanes can behave as blockages. For the sake of tractability, our theoretical model tractable will consider the service of a *standard user* placed at the origin $O = (0, 0)$ of the axis.

A. BS-Standard User Association and Antenna Model

Since vehicles in the slow lanes can block a direct link between the standard user and each BS, it is necessary to distinguish between BSs that are in LOS with the standard user and those that are in NLOS. BS i is said to be in LOS if the footprint of any blockage does not intersect with the direct ray from the standard user. The probability that BS i is in LOS is denoted by $p_{i,\mathrm{L}}$. We assume that the blockages are of length τ, illustrated in Fig. 1. In the case that the direct ray is blocked, BS i is in NLOS and this occurs with probability $p_{i,\mathrm{N}}$ and the relation $p_{i,\mathrm{N}} = 1-p_{i,\mathrm{L}}$ holds. By Assumption 3.3, we observe that the probability $p_{i,\mathrm{E}}$ for $\mathrm{E} \in \{\mathrm{L}, \mathrm{N}\}$ of BS i being in LOS ($\mathrm{E} = \mathrm{L}$) or NLOS ($\mathrm{E} = \mathrm{N}$) depends on the distance from O. This is due to the fact that the further the BS is from the user, the further away the center of an obstacle footprint segment needs to be to avoid a blockage.

Consider Assumption 3.3 and the set of points where the segment connecting O with BS i intersects the symmetry axis of each obstacle lane. We approximate $p_{i,\mathrm{L}}$ with the probability p_{L} that no blockages are present within a distance of $\tau/2$ on either side of the ray connecting the user to BS i. Hence, our approximation is independent of the distance from BS i to O and $p_{i,\mathrm{L}}$ can be approximated independently of i as follows:

$$p_{\mathrm{L}} \cong \prod_{\ell=1}^{N_o} e^{-\lambda_{\mathrm{o},\ell}\tau}, \tag{1}$$

while $p_{i,\mathrm{N}}$ is approximated as $p_{\mathrm{N}} = 1 - p_{\mathrm{L}}$. Observe also that the term $e^{-\lambda_{\mathrm{O},\ell}\tau}$ is the void probability of a one-dimensional PPP of density $\lambda_{\mathrm{o},\ell}$ [41].

Using the approximation in (1) and invoking the independent thinning theorem of PPP, it follows that the PPP of the LOS BSs $\Phi_{\mathrm{L}} \subseteq \Phi_{\mathrm{BS}}$ and of the NLOS BS $\Phi_{\mathrm{N}} \subseteq \Phi_{\mathrm{BS}}$ are independent and with density $\lambda_{\mathrm{L}} = p_{\mathrm{L}}\lambda_{\mathrm{BS}}$ and $\lambda_{\mathrm{N}} = p_{\mathrm{N}}\lambda_{\mathrm{BS}}$, respectively. In addition, the relation $\Phi_{\mathrm{L}} \cap \Phi_{\mathrm{N}} = \emptyset$ holds.

Consider the i-th BS at a distance $r_i = \sqrt{x_i^2 + y_i^2}$ from the standard user. The indicator function $\mathbf{1}_{i,\mathrm{L}}$ is equal to one if BS i is in LOS with respect to the standard user, and zero otherwise. The path loss component $\ell(r_i)$ impairing the signal transmitted by BS i and received by the standard user is defined as follows:

$$\ell(r_i) = \mathbf{1}_{i,\mathrm{L}} C_{\mathrm{L}} r_i^{-\alpha_{\mathrm{L}}} + (1 - \mathbf{1}_{i,\mathrm{L}}) C_{\mathrm{N}} r_i^{-\alpha_{\mathrm{N}}} \tag{2}$$

where α_{L} and α_{N} are the path loss exponents, while C_{L} and C_{N} are the path loss intercept factors in the LOS and NLOS cases, respectively. From Assumption 3.1, we remark that relation $r_i \geq w(N_o + 1)$ holds. Hence, for typical values of road lane widths, path loss intercept factors and exponents,

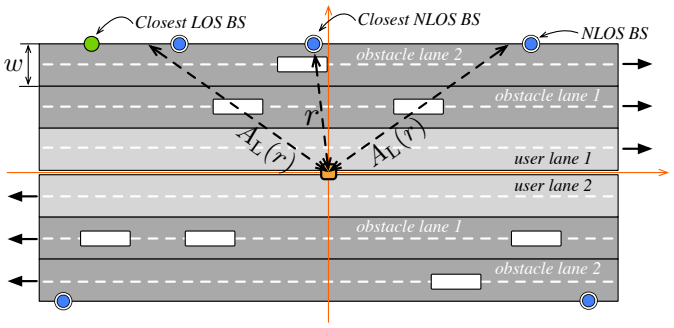

Fig. 2. Proposed BS-standard user association model. In this case, the standard user connects to a NLOS BS.

relation $w(N_o + 1) \geq \max\{C_{\mathrm{L}}^{\frac{1}{\alpha_{\mathrm{L}}}}, C_{\mathrm{N}}^{\frac{1}{\alpha_{\mathrm{N}}}}\}$ holds as well[2]. This ensures that both $C_{\mathrm{L}} r_i^{-\alpha_{\mathrm{L}}}$ and $C_{\mathrm{N}} r_i^{-\alpha_{\mathrm{N}}}$ are less than or equal to 1.

Assumption 3.4 (BS-Standard User Association): In our system model, the standard user has perfect channel state information and always connects to the BS with index i^*, which is characterized by the minimum path loss component, i.e., $i^* = \arg\max_{i=1,\ldots,b} \{\ell(r_i)\}$.

We assume that the standard user connects to a NLOS BS at a distance r. Since $w(N_o+1) \geq \max\{C_{\mathrm{L}}^{\frac{1}{\alpha_{\mathrm{L}}}}, C_{\mathrm{N}}^{\frac{1}{\alpha_{\mathrm{N}}}}\}$, it follows that there are no LOS BSs at a distance less than or equal to $A_{\mathrm{L}}(r)$, defined as:

$$A_{\mathrm{L}}(r) = \max\left\{ w(N_o+1), \left[\frac{C_{\mathrm{N}}}{C_{\mathrm{L}}} r^{-\alpha_{\mathrm{N}}}\right]^{-\frac{1}{\alpha_{\mathrm{L}}}} \right\}. \tag{3}$$

We observe that $A_{\mathrm{L}}(r)$ is the distance from O for which the path loss component associated with a LOS BS is equal to the path loss component associated with a NLOS BS at a distance r. In a similar way, we observe that if the standard user connects to a LOS BS at a distance r from O, it follows that there are no NLOS BSs at a distance smaller than or equal to $A_{\mathrm{N}}(r)$, defined as:

$$A_{\mathrm{N}}(r) = \max\left\{ w(N_o+1), \left[\frac{C_{\mathrm{L}}}{C_{\mathrm{N}}} r^{-\alpha_{\mathrm{L}}}\right]^{-\frac{1}{\alpha_{\mathrm{N}}}} \right\}. \tag{4}$$

We observe that definitions (3) and (4) prevent $A_{\mathrm{L}}(r)$ and $A_{\mathrm{N}}(r)$ to be smaller than the distance $w(N_o+1)$ between O and a side of the road.

The standard user will always connect to one BS at a time, which is either the closest LOS or the closest NLOS BS. This choice is made by the standard user according to Assumption 3.4. For instance, Fig. 2 shows the case where the closest LOS BS is at a distance greater than $\mathrm{A_L}(r)$. In this case, the BS associated with the smallest path loss component is the closest NLOS BS, which is at a distance r to the standard user. Those facts allow us to prove the following lemma.

Lemma 3.1: Let $\mathrm{d_L}$ and $\mathrm{d_N}$ be the random variables expressing the distance to the closest LOS and NLOS BSs from the

[2]For instance, we observe that the relation holds for any path loss exponent if $C_{\mathrm{L}} = 1$, $C_{\mathrm{N}} = 1$ and $w(N_0 + 1) \geq 1$ m.

perspective of the standard user, respectively. The Probability Density Function (PDF) of $\mathrm{d_L}$ can be expressed as:

$$f_{\mathrm{L}}(r) = \frac{2\lambda_{\mathrm{L}} r}{b(r)} e^{-2\lambda_{\mathrm{L}} b(r)}, \tag{5}$$

while the PDF of $\mathrm{d_N}$ can be expressed as

$$f_{\mathrm{N}}(r) = \frac{2\lambda_{\mathrm{N}} r}{b(r)} e^{-2\lambda_{\mathrm{N}} b(r)}, \tag{6}$$

where $b(r) = \sqrt{r^2 - w^2(N_o+1)^2}$.

Proof: Considering the LOS case, the proof directly follows from the expression of the PDF of the distance of the closest point to the origin of the axis in a one-dimensional PPP with density λ_{L}, which is $f_{\mathrm{L}}(t) = 2\lambda_{\mathrm{L}} e^{-2\lambda_{\mathrm{L}} t}$ [41, Eq. (2.12)]. By applying the change of variable $t \leftarrow b(r)$ we obtain (5). With similar reasoning, it is also possible to prove (6). ■

Using Lemma 3.1, (3) and (4), the following lemma holds.

Lemma 3.2: The standard user connects to a NLOS BS with probability

$$\mathrm{P_N} = \int_{w(N_o+1)}^{\infty} f_{\mathrm{N}}(r) e^{-2\lambda_{\mathrm{L}} b(A_{\mathrm{L}}(r))}\, dr. \tag{7}$$

On the other hand, the standard user connects to a LOS BS with probability

$$\mathrm{P_L} = \int_{w(N_o+1)}^{\infty} f_{\mathrm{L}}(r) e^{-2\lambda_{\mathrm{N}} b(A_{\mathrm{N}}(r))}\, dr = 1 - \mathrm{P_N}. \tag{8}$$

Proof: Consider the event that the standard user connects to a NLOS BS, which is at a distance r from O. This event is equivalent of having all the LOS BSs at a distance greater than or equal to $A_{\mathrm{L}}(r)$. From (5), it follows that $\mathbb{P}[\mathrm{d_L} \geq A_{\mathrm{L}}(r) \text{ and } \mathrm{d_N} = r]$ is equal to $e^{-2\lambda_{\mathrm{L}} b(A_{\mathrm{L}}(r))}$. Then if we marginalize $\mathbb{P}[\mathrm{d_L} \geq A_{\mathrm{L}}(r) \text{ and } \mathrm{d_N} = r]$ with respect to r, we obtain (7). The same reasoning applies to the proof of (8). ■

The gain of the signal received by the standard user depends on the antenna pattern and beam steering performed by the BS and the user. Each BS and the standard user are equipped with antenna arrays capable of performing directional beamforming. To capture this feature, we follow [21] and use a sectored approximation to the array pattern. We detail the sectored approximation for our highway model in the following assumption.

Assumption 3.5 (Antenna Pattern): The antenna pattern consists of a main lobe with beamwidth ψ and a side lobe that covers the remainder of the antenna pattern. We assume that the gain of the main lobe is G_{TX} and the gain of the sidelobe is g_{TX}. Similarly, the antenna pattern of the standard user also consists of main lobe with beamwidth ψ and gain G_{RX}, and a side lobe with gain g_{RX}.

The antenna of each BS and the user can be steered as follows.

Assumption 3.6 (BS Beam Steering): Let ϵ_i be the angle between the upper (bottom) side of the road and the antenna boresight of BS i (see Fig. 1). We assume that ϵ_i takes values in $\mathcal{G} = [\frac{\psi}{2}, 2\pi - \frac{\psi}{2}]$. As such, the main lobe of each BS is always entirely directed towards the road portion constrained by the upper and bottom side. If the standard user connects to BS i, the BS steers its antenna beam towards the standard user. On the other hand, if the standard user is not connected to BS i, we assume that ϵ_i takes a value that is uniformly distributed in $\mathcal{G}$.

Assumption 3.7 (Standard User Beam Steering): The angle $\epsilon^{(U)}$ between the positive x-axis and the boresight of the user beam is selected to maximize the gain of the received signal from the serving BS. We assume that $\epsilon^{(U)} \in [\frac{\psi}{2}, \pi - \frac{\psi}{2}]$ or $\epsilon^{(U)} \in [\pi + \frac{\psi}{2}, 2\pi - \frac{\psi}{2}]$ if the user is served by a BS on the upper side or the bottom side of the road respectively. This assumption ensures that interfering BSs on the opposite side of the road are always received by a sidelobe, with gain g_{RX}. We also assume that the standard user directs its antenna beam towards the serving BS, which is then received with gain G_{RX}.

IV. SINR Outage and Rate Coverage Characterization

For the sake of simplifying the notation and without loss of generality, we assume that the BS with index 1 is the BS that the standard user is connected to, while BSs $2, \ldots, b$ define the set of the interfering BSs. We define the SINR at the location of the standard user as follows:

$$\mathrm{SINR}_O = \frac{|h_1|^2\, \Delta_1\, \ell(r_1)}{\sigma + \mathrm{I}}, \tag{9}$$

where

$$\mathrm{I} = \sum_{j=2}^{b} |h_j|^2\, \Delta_j\, \ell(r_j). \tag{10}$$

Terms h_i and Δ_i are the small-scale fading component and the overall transmit/receive antenna gain associated with BS i, respectively, for $i = 1, \ldots, b$. The term I is the total interference contribution determined by all the BSs except the one connected to the standard user, i.e., the total interference determined by BSs $2, \ldots, b$. From Assumption 3.6 and 3.7, it follows that Δ_1 is equal to $G_{\mathrm{TX}} G_{\mathrm{RX}}$. Finally, σ represents the thermal noise power normalized with respect to the transmission power P_t.

As acknowledged in [7] there is a lack of extensive measurements for vehicular mmWave networks, as well as widely accepted channel models. Therefore, it is necessary to adopt conservative assumptions on signal propagation. As summarized in Table II, several channel models have been proposed in the literature. Typically publicly available system-level mmWave simulators [42] adopt channel models entirely [21] or partially [29] based on the Nakagami model, which are more refined alternatives to the widely adopted models dictating constant small-scale contributions [27], [28], [31]. In particular, we adopt the same channel model in [29], which is based on the following observations: (i) because of the beamforming capabilities and the sectorial antenna pattern, the signal is impaired only by a limited number of scatterers, and (ii) the interfering transmissions cluster with many scatterers and reach the standard user. Furthermore, the considered sectorial antennal model at the transmitter and receiver sides (see Assumption 3.5) significantly reduces the angular spread of the incoming signals – thus reducing the Doppler spread. Moreover, the incoming signals are concentrated in one direction. Hence, it is likely that there

is a non-zero bias in the Doppler spectrum, which can be compensated by the automatic frequency control loop at the receiver side [43]. For these reasons, the Doppler effect has been assumed to be mitigated.

Assumption 4.1 (Channel Model): The channel between the serving BS and standard user is described by a Nakagami channel model with parameter m, and hence, $|h_1|^2$ follows a gamma distribution (with shape parameter m and rate equal to 1). On the other hand, to capture the clustering of interfering transmissions the channels between the standard user and each interfering BS are modelled as independent Rayleigh channels – thus $|h_2|^2, \ldots, |h_b|^2$ are independently and identically distributed as an exponential distribution with mean equal to 1.

A. Analytical Characterization of I

In order to provide an analytical characterization of the interference power at O, it is convenient to split the term I into four different components: (i) $\mathrm{I}_{\mathrm{U,L}}$ and $\mathrm{I}_{\mathrm{U,N}}$ representing the interference power associated with LOS and NLOS BSs placed on the upper side of the road whose positions are defined by the PPPs $\Phi_{\mathrm{U,L}}$ and $\Phi_{\mathrm{U,N}}$, respectively, and, (ii) $\mathrm{I}_{\mathrm{B,L}}$ and $\mathrm{I}_{\mathrm{B,N}}$ the interference power generated by LOS and NLOS BSs on the bottom side of the road placed at the location given by the PPPs $\Phi_{\mathrm{B,L}}$ and $\Phi_{\mathrm{B,N}}$. Overall, the total interference power is given by $\mathrm{I} = \sum_{\mathrm{S}\in\{\mathrm{U,B}\},\mathrm{E}\in\{\mathrm{L,N}\}} \mathrm{I}_{\mathrm{S,E}}$. In addition, the relations $\Phi_{\mathrm{L}} = \Phi_{\mathrm{U,L}} \bigcup \Phi_{\mathrm{B,L}}$ and $\Phi_{\mathrm{N}} = \Phi_{\mathrm{U,N}} \bigcup \Phi_{\mathrm{B,N}}$ hold.

In the following result, we derive an approximation for the Laplace transform $\mathcal{L}_{\mathrm{I}}(s)$ of I.

Theorem 4.1: Let $\mathbb{S}_1 = \mathrm{U}$ and $\mathbb{S}_1 = \mathrm{B}$ represent the cases where the standard user connects to a BS on the upper or the bottom side of the road, respectively. In addition, let $\mathbb{E}_1 = \mathrm{L}$ and $\mathbb{E}_1 = \mathrm{N}$ signify the cases where the standard user connects to a LOS or NLOS BS, respectively. The Laplace transform $\mathcal{L}_{\mathrm{I_{S,E}},\mathbb{E}_1}(s)$ of $\mathrm{I_{S,E}}$, conditioned on $\mathbb{E}_1$, for $\mathrm{S} \in \{\mathrm{U,B}\}$ and $\mathrm{E} \in \{\mathrm{L,N}\}$, can be approximated as follows:

$$\mathcal{L}_{\mathrm{I_{S,E}},\mathbb{E}_1}(s) \cong \prod_{\substack{\mathbb{S}_1\in\{\mathrm{U,B}\},\\ (a,b,\Delta)\in\mathcal{C}_{|\mathrm{x_1}|,\mathbb{S}_1,\mathbb{E}_1,\mathrm{S,E}}}} \sqrt{\mathcal{L}_{\mathrm{I_{S,E}},\mathbb{E}_1}(s;a,b,\Delta)}, \tag{11}$$

where $\mathcal{L}_{\mathrm{I_{S,E}},\mathbb{E}_1}(s;a,b,\Delta)$ is defined as in (31). We define the x-axis coordinates J and K of the points where the two rays defining the standard user beam intersect with a side of the road, as $J = w(N_o+1)/[\tan(\epsilon^{(\mathrm{U})} + \psi/2)]$ and $K = w(N_o+1)/[\tan(\epsilon^{(\mathrm{U})} - \psi/2)]$, where $\epsilon^{(\mathrm{U})} = \tan^{-1}[w(N_o+1)/x_1]$ (see Fig. 10). Furthermore, let us define $x_{\mathrm{L}}(r_1) = \sqrt{(\mathrm{A_L}(r_1))^2 - w^2(N_o+1)^2}$ and $x_{\mathrm{N}}(r_1) = \sqrt{(\mathrm{A_N}(r_1))^2 - w^2(N_o+1)^2}$. Different combinations of parameters $< |\mathrm{x_1}|, \mathbb{S}_1, \mathbb{E}_1, \mathrm{S}, \mathrm{E} >$ determine different sequences $\mathcal{C}_{|\mathrm{x_1}|,\mathbb{S}_1,\mathbb{E}_1,\mathrm{S,E}}$ of parameter configurations (a,b,Δ), as defined in Table IV.

Proof: See Appendix A. ∎

Example 4.1: Consider the scenario where the standard user connects to a LOS BS, i.e., $\mathbb{E}_1 = \mathrm{L}$, and relation $J > 0$ holds. We evaluate the Laplace transform of the interference associated with the BSs located on the upper side of the road ($\mathrm{S} = \mathrm{U}$) that are in LOS with respect to the standard user ($\mathrm{E} = \mathrm{L}$). The sequence $\mathcal{C}_{|\mathrm{x_1}|,\mathrm{U,L,U,L}}$ is given by the first row of Table IV, while $\mathcal{C}_{|\mathrm{x_1}|,\mathrm{B,L,U,L}}$ consists of the same elements of sequence $\mathcal{C}_{|\mathrm{x_1}|,\mathrm{U,L,B,L}}$ (last row of Table IV). As a result, $\mathcal{L}_{\mathrm{I_{S,E}},\mathbb{E}_1}(s)$ can be approximated as follows:

$$\begin{aligned}\mathcal{L}_{\mathrm{I_{S,E}},\mathbb{E}_1}(s) \cong \Big[&\mathcal{L}_{\mathrm{I_{S,E}},\mathbb{E}_1}(s;|x_1|,K,g_{\mathrm{TX}}G_{\mathrm{RX}}) \\ &\cdot \mathcal{L}_{\mathrm{I_{S,E}},\mathbb{E}_1}(s;K,+\infty,g_{\mathrm{TX}}g_{\mathrm{RX}}) \\ &\cdot \mathcal{L}_{\mathrm{I_{S,E}},\mathbb{E}_1}(s;|x_1|,+\infty,g_{\mathrm{TX}}g_{\mathrm{RX}})\Big]^{1/2} \\ &\cdot \mathcal{L}_{\mathrm{I_{S,E}},\mathbb{E}_1}(s;x_{\mathrm{N}}(r_1),+\infty,g_{\mathrm{TX}}g_{\mathrm{RX}}).\end{aligned} \tag{12}$$

From Theorem 4.1 and the fact that I is defined as a sum of statistically independent interference components, the following corollary holds.

Corollary 4.1: The Laplace transform of I, for $\mathbb{E}_1 = \{\mathrm{L,N}\}$, can be approximated as follows:

$$\mathcal{L}_{\mathrm{I},\mathbb{E}_1}(s) \cong \prod_{\mathrm{S}\in\{\mathrm{U,B}\},\mathrm{E}\in\{\mathrm{L,N}\}} \mathcal{L}_{I_{\mathrm{S,E}},\mathbb{E}_1}(s) \tag{13}$$

Example 4.2: Consider the scenario where $\mathbb{E}_1 = \mathrm{L}$, and relation $J > 0$ holds. Using Corollary 4.1, $\mathcal{L}_{\mathrm{I_{S,E}},\mathbb{E}_1}(s)$ can be approximated as follows:

$$\begin{aligned}\mathcal{L}_{\mathrm{I},\mathbb{E}_1}(s) \cong\ &\mathcal{L}_{\mathrm{I_{S,E}},\mathbb{E}_1}(s;|x_1|,K,g_{\mathrm{TX}}G_{\mathrm{RX}}) \\ &\cdot \mathcal{L}_{\mathrm{I_{S,E}},\mathbb{E}_1}(s;x_{\mathrm{N}}(r_1),J,g_{\mathrm{TX}}g_{\mathrm{RX}}) \\ &\cdot \mathcal{L}_{\mathrm{I_{S,E}},\mathbb{E}_1}(s;J,K,g_{\mathrm{TX}}G_{\mathrm{RX}}) \\ &\cdot \left(\mathcal{L}_{\mathrm{I_{S,E}},\mathbb{E}_1}(s;K,+\infty,g_{\mathrm{TX}}g_{\mathrm{RX}})\right)^2 \\ &\cdot \left(\mathcal{L}_{\mathrm{I_{S,E}},\mathbb{E}_1}(s;|x_1|,+\infty,g_{\mathrm{TX}}g_{\mathrm{RX}})\right)^3 \\ &\cdot \left(\mathcal{L}_{\mathrm{I_{S,E}},\mathbb{E}_1}(s;x_{\mathrm{N}}(r_1),+\infty,g_{\mathrm{TX}}g_{\mathrm{RX}})\right)^3\end{aligned} \tag{14}$$

TABLE IV
VALUES OF (a,b,Δ) FOR DIFFERENT $< |\mathrm{x_1}|, \mathbb{S}_1, \mathbb{E}_1, \mathrm{S}, \mathrm{E} >$.

Configuration of $< \mathbb{S}_1, \mathbb{E}_1, \mathrm{S}, \mathrm{E} >$	**Conditions on** $\lvert x_1\rvert$	**Enumeration of elements** $(a,b,\Delta) \in \mathcal{C}_{\lvert \mathrm{x_1}\rvert,\mathbb{S}_1,\mathbb{E}_1,\mathrm{S,E}}$
$< \mathrm{U,L,U,L} >$	For any $\lvert x_1\rvert$ such that $J > 0$	$(\lvert x_1\rvert, K, g_{\mathrm{TX}}G_{\mathrm{RX}})$, $(K, +\infty, g_{\mathrm{TX}}g_{\mathrm{RX}})$, $(\lvert x_1\rvert, +\infty, g_{\mathrm{TX}}g_{\mathrm{RX}})$
	For any $\lvert x_1\rvert$ such that $J \leq 0$	$(\lvert x_1\rvert, K, g_{\mathrm{TX}}G_{\mathrm{RX}})$, $(K, +\infty, g_{\mathrm{TX}}g_{\mathrm{RX}})$, $(\lvert x_1\rvert, \lvert J\rvert, g_{\mathrm{TX}}G_{\mathrm{RX}})$, $(\lvert J\rvert, +\infty, g_{\mathrm{TX}}g_{\mathrm{RX}})$
$< \mathrm{U,L,U,N} >$	For any $\lvert x_1\rvert$ such that $J > 0$	$(x_{\mathrm{N}}(r_1), J, g_{\mathrm{TX}}g_{\mathrm{RX}})$, $(x_{\mathrm{N}}(r_1), +\infty, g_{\mathrm{TX}}g_{\mathrm{RX}})$, $(J, K, g_{\mathrm{TX}}G_{\mathrm{RX}})$, $(K, +\infty, g_{\mathrm{TX}}g_{\mathrm{RX}})$
	For any $\lvert x_1\rvert$ such that $J \leq 0$	Refer to the case $< \mathrm{U,L,U,L} > (J \leq 0)$ and replace $\lvert x_1\rvert$ with $x_{\mathrm{N}}(r_1)$
$< \mathrm{U,L,B,L} >$	For any $\lvert x_1\rvert$	$(\lvert x_1\rvert, +\infty, g_{\mathrm{TX}}g_{\mathrm{RX}})$, $(\lvert x_1\rvert, +\infty, g_{\mathrm{TX}}g_{\mathrm{RX}})$,
$< \mathrm{U,L,B,N} >$	Refer to the case $< \mathrm{U,L,B,L} >$ and replace $\lvert x_1\rvert$ with $x_{\mathrm{N}}(r_1)$	
$< \mathrm{U,N,U,L} >$	For any $\lvert x_1\rvert$ such that $x_{\mathrm{L}}(r_1) > K$	Refer to the case $< \mathrm{U,L,B,L} >$ and replace $\lvert x_1\rvert$ with $x_{\mathrm{L}}(r_1)$
	For any $\lvert x_1\rvert$ such that $x_{\mathrm{L}}(r_1) \leq K$	Refer to the case $< \mathrm{U,L,U,L} >$ and replace $\lvert x_1\rvert$ with $x_{\mathrm{L}}(r_1)$
$< \mathrm{U,N,U,N} >$	Refer to the case $< \mathrm{U,L,U,L} >$	
$< \mathrm{U,N,B,L} >$	Refer to the case $< \mathrm{U,L,B,L} >$ and replace x_1 with $x_{\mathrm{L}}(r_1)$	
$< \mathrm{U,N,B,N} >$	Refer to the case $< \mathrm{U,L,B,L} >$	
Cases where $\mathbb{S}_1 = \mathrm{B}$, $\mathrm{S} = \mathrm{B}$	Refer to the correspondent cases where $\mathbb{S}_1 = \mathrm{U}$ and $\mathrm{S} = \mathrm{U}$	
Cases where $\mathbb{S}_1 = \mathrm{B}$, $\mathrm{S} = \mathrm{U}$	Refer to the correspondent cases where $\mathbb{S}_1 = \mathrm{U}$ and $\mathrm{S} = \mathrm{B}$	

B. SINR Outage and Rate Coverage Probability Framework

The general framework for evaluating the SINR outage probability is given in the following result.

Theorem 4.2: Let

$$\mathrm{F_L}(t) = e^{-2\lambda_\mathrm{L}\sqrt{t^2-w^2(N_o+1)^2}} \tag{15}$$

and

$$\mathrm{F_N}(t) = e^{-2\lambda_\mathrm{N}\sqrt{t^2-w^2(N_o+1)^2}} \tag{16}$$

be the probability of a LOS or NLOS BS not being at a distance smaller than t from O, respectively. We regard $\mathrm{P_T}(\theta)$ to be the SINR outage probability with respect to a threshold θ, i.e., the probability that SINR_O is smaller than a threshold θ. $\mathrm{P_T}(\theta)$ can be expressed as follows:

$$\mathrm{P_T}(\theta) = \mathrm{P_L} - \overbrace{\mathbb{P}[\mathrm{SINR}_O > \theta \wedge \text{std. user served in LOS}]}^{\mathrm{P_{CL}}(\theta)} + \mathrm{P_N} - \underbrace{\mathbb{P}[\mathrm{SINR}_O > \theta \wedge \text{std. user served in NLOS}]}_{\mathrm{P_{CN}}(\theta)} \tag{17}$$

where

$$\mathrm{P_{CL}}(\theta) = \Big|_{\mathbb{E}_1=\mathrm{L}} - \sum_{k=0}^{m-1}(-1)^{m-k}\binom{m}{k}\int_{w(N_o+1)}^{+\infty} e^{-\frac{v\sigma\theta(m-k)}{\Delta_1\mathrm{C_L}}r_1^{\alpha_\mathrm{L}}} \cdot \mathcal{L}_{\mathrm{I},\mathbb{E}_1}\left(\frac{v\theta r_1^{\alpha_\mathrm{L}}(m-k)}{\Delta_1\mathrm{C_L}}\right) f_\mathrm{L}(r_1)\mathrm{F_N}(\mathrm{A_N}(r_1))\,dr_1 \tag{18}$$

and

$$\mathrm{P_{CN}}(\theta) = \Big|_{\mathbb{E}_1=\mathrm{N}} - \sum_{k=0}^{m-1}(-1)^{m-k}\binom{m}{k}\int_{w(N_o+1)}^{+\infty} e^{-\frac{v\sigma\theta(m-k)}{\Delta_1\mathrm{C_N}}r_1^{\alpha_\mathrm{N}}} \cdot \mathcal{L}_{\mathrm{I},\mathbb{E}_1}\left(\frac{v\theta r_1^{\alpha_\mathrm{N}}(m-k)}{\Delta_1\mathrm{C_N}}\right) f_\mathrm{N}(r_1)\mathrm{F_L}(\mathrm{A_L}(r_1))\,dr_1, \tag{19}$$

represent the probability of the standard user not experiencing SINR outage while connected to a LOS or NLOS BS, respectively.

Proof: The result (17) follows immediately once $\mathrm{P_{CL}}(\theta)$ and $\mathrm{P_{CN}}(\theta)$ as known. In particular, the following relation holds (for $\mathbb{E}_1 = \mathrm{L}$):

$$\begin{aligned}\mathrm{P_{CL}}(\theta) &= \mathbb{P}\left[\frac{|h_1|^2\,\Delta_1\,\ell(r_1)}{\sigma+\mathrm{I}} > \theta \wedge \text{std. user served in LOS}\right] \\ &\overset{(i)}{\cong} \mathbb{E}_\mathrm{I}\int_{w(N_o+1)}^{+\infty}\left(1-\left(1-e^{-v\frac{(\sigma+\mathrm{I})\theta}{\Delta_1\mathrm{C_L}}r_1^{\alpha_\mathrm{L}}}\right)^m\right) \cdot f_\mathrm{L}(r_1)\mathrm{F_N}(\mathrm{A_N}(r_1))\,dr_1\end{aligned} \tag{20}$$

where $v = m(m!)^{-1/m}$ [21, Lemma 6] and (i) arise from $|h_1|^2$ being distributed as a gamma random variable. In addition, $\mathrm{F_N}(\mathrm{A_N}(r_1))$ is defined as the probability of a NLOS BS not being at a distance smaller than $\mathrm{A_N}(r_1)$ to O, i.e., the probability that the standard user is not connected to a NLOS BS. The expression of $\mathrm{F_N}(t)$, as in (16), immediately follows from the simplification of the following relation:

$$\mathrm{F_N}(t) = 1 - \int_{w(N_o+1)}^{t} f_\mathrm{N}(r)\,dr. \tag{21}$$

From the binomial theorem, we swap the integral and the expectation with respect to I and invoke Corollary 4.1 to obtain (18). By following the same reasoning, it is also possible to derive expressions for $\mathrm{P_{CN}}(\theta)$ and $\mathrm{F_L}(t)$. ■

As the value of α_N increases it is less likely that the standard user connects to a NLOS BS. This intuition can be readily confirmed from (17) as follows.

Remark 4.1: From (4), A_N is likely to be equal to $w(N_o+1)$, for large values of α_N. As a result, the exponential term in (8) approaches one and, hence, $\mathrm{P_L}$ can be approximated as follows:

$$\mathrm{P_L} \cong \int_{w(N_o+1)}^{\infty} f_\mathrm{L}(r)\,dr = \int_0^{\infty} 2\lambda_\mathrm{L}e^{-2\lambda_\mathrm{L}t} = 1. \tag{22}$$

Using this approximation, it follows that $\mathrm{P_N} \cong 0$ holds. In addition, since $\mathrm{P_{CN}}$ is always less than or equal to $\mathrm{P_N}$, the relation $\mathrm{P_{CN}} \cong 0$ holds as well. If $A_\mathrm{N} \cong w(N_o+1)$, the relation $\mathrm{F_N}(\mathrm{A_N}(r_1)) \cong 1$ holds. For these reasons, $\mathrm{P_T}(\theta)$ can be approximated as follows:

$$\mathrm{P_T}(\theta) \cong 1 + \sum_{k=0}^{m-1}(-1)^{m-k}\binom{m}{k}\int_{w(N_o+1)}^{+\infty} e^{-\frac{v\sigma\theta(m-k)}{\Delta_1\mathrm{C_L}}r_1^{\alpha_\mathrm{L}}} \cdot \mathcal{L}_{\mathrm{I},\mathbb{E}_1}\left(\frac{v\theta r_1^{\alpha_\mathrm{L}}(m-k)}{\Delta_1\mathrm{C_L}}\right) f_\mathrm{L}(r_1)\,dr_1. \tag{23}$$

From [40, Theorem 1] and by using Theorem 4.2, it is now possible to express the rate coverage probability $\mathrm{R_C}(\kappa)$, i.e., the probability that the standard user experiences a rate that is greater than or equal to κ. In particular, the rate coverage probability is given by:

$$\begin{aligned}\mathrm{R_C}(\kappa) &= \mathbb{P}[\text{rate of std. user} \geq \kappa] \\ &= 1 - \mathrm{P_T}(2^{\kappa/W}-1),\end{aligned} \tag{24}$$

where W is the system bandwidth.

V. Numerical Results

A. Simulation Framework

In this section, we validate the proposed theoretical model against simulated highway scenarios. We remark that Assumption 3.1 models the highway as infinitely long, which is not possible in a simulation. However, as noted in [44], [45], the radius R of the simulated system (i.e., the length of the simulated road section $2R$) can be related to the simulation accuracy error ε, as in [44, Eq. (3.5)]. In the case of a one-dimensional PPP, the radius is related to the simulation error by $R \geq \varepsilon^{-\frac{1}{\alpha_\mathrm{L}-1}}$.

We simulated scenarios where the standard user drives on the lower-most user lane along with multiple other vehicles; in particular, we considered a number of vehicles equal to $\lfloor 2R\lambda_u \rfloor$, where λ_u is the vehicle density driving on each user lane. In addition, a number of blockages equal to $\lfloor 2R\lambda_{o,i} \rfloor$ are placed at random on each obstacle lane i, for $i = 1, \ldots, N_o$. During each simulated scenario, both the vehicles driving on the user lanes and blockages move according to the Krauss car-following mobility model [46] and their maximum speed is set equal to $70\,\mathrm{mph}$ (i.e., $112\,\mathrm{km\,h^{-1}}$) and $60\,\mathrm{mph}$ (i.e., $96\,\mathrm{km\,h^{-1}}$), respectively as dictated by the current British speed limits[3]. In order to keep the density of the simulated

[3]We refers to the Highway Code (https://www.gov.uk/speed-limits) valid for England, Scotland and Wales.

TABLE V
MAIN SIMULATION PARAMETERS.

Parameter	Value
Simulated time	13 h (for Figs. 4-8), 55 h (for Figs. 3 and 9)
Length of the simulated road section (i.e., $2R$)	20 km, 100 km
w	3.7 m, as per [48]
λ_u	$2 \cdot 10^{-2}$
Mobility model	Blockages and the standard user move according to a Krauss car-following mobility model [46]; maximum acceleration and deceleration equal to $5.3\,\mathrm{m/s^2}$ [49], maximum vehicle speed equal to $96\,\mathrm{km\,h^{-1}}$ (blockages) and $112\,\mathrm{km\,h^{-1}}$ (standard user).
Blockage dimensions	The dimensions of a double decker bus, i.e., length τ equal to 11.2 m and width equal to 2.52 m [50]
N_o	1, 2
$\{\lambda_{o,1}, \lambda_{o,2}\}$	$\{1 \cdot 10^{-2}, 2 \cdot 10^{-2}\}$, i.e., one blockage every $\{100\,\mathrm{m}, 50\,\mathrm{m}\}$
λ_{BS}	From $2 \cdot 10^{-4}$ to $1 \cdot 10^{-2}$, with a step of $2 \cdot 10^{-4}$
$\mathrm{C_L}$, $\mathrm{C_N}$	1
α_{L}	2.8
α_{N}	3.86
m	3, as per [29]
ϕ	$\{30^\circ, 90^\circ\}$
G_{TX}	$\{10\,\mathrm{dB}, 20\,\mathrm{dB}\}$
G_{RX}	10 dB
g_{TX}, g_{RX}	-10 dB
W	100 MHz
P_t	27 dBm
Thermal noise power (i.e, $\sigma \cdot P_t$)	$10\log_{10}(k \cdot T \cdot W \cdot 10^3)$ dBm, where k is the Boltzmann constant and the temperature $T = 290$ K [16]

blockages constant and hence allow a fair validation of the proposed theoretical framework, we adopted the Krauss car-following mobility model with the wrap-around policy [47]. In particular, when a vehicle reaches the end of the simulated road section, it re-enters at the beginning.

BSs are positioned uniformly at random at both sides of the road. The simulator estimates the SINR outage probability $\mathrm{P_T}$ and rate coverage probability $\mathrm{R_C}$ by averaging over the total simulation time and across a number of BS random locations and steering angle configurations (of the interfering BSs); number allowing to the simulated average performance metrics to converge to a stable value. We remark that the adoption of highly directional antennas significantly reduces the angular spread of the incoming signals. As such, in the simulated scenarios, we assume the standard user is equipped with an automatic frequency control loop compensating for the Doppler effect [43]. In addition, the simulated channel follows Assumption 4.1. This allows us to validate the proposed model in propagation conditions that are compatible to publicly available system-level mmWave simulators and analytical investigations [29], [42].

With regards to Table V, we consider $N_o = \{1, 2\}$ obstacle lanes per driving direction. For $N_o = 2$, we assume different traffic intensities by setting densities $\{\lambda_{\mathrm{o},1}, \lambda_{\mathrm{o},2}\}$ as per row six of Table V. Furthermore, we consider a typical highway lane width w [48].

In order to effectively validate the proposed BS-standard user association scheme, we avoided scenarios where it was unlikely for the standard user to connect to a NLOS BS (see Remark 4.1), such as $\alpha_{\mathrm{N}} \geq 5.76$. To this end, we set the path loss exponents $\alpha_{\mathrm{L}} = 2.8$ and $\alpha_{\mathrm{N}} = 3.86$, which are realistic values for mmWave links [17]. In Section III-A, we

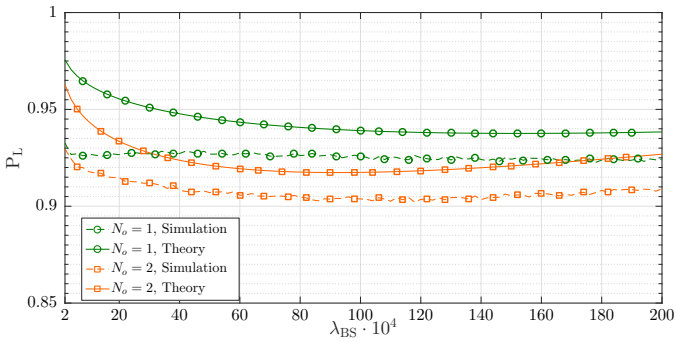

Fig. 3. Probability $\mathrm{P_L}$ that the standard users connects to a LOS BS as a function of λ_{BS}, for $N_o = 1$ and 2.

approximated the probabilities p_{L} and p_{N} for a BS of being in LOS or NLOS with respect to the standard user, respectively. It is worth noting that approximation (1) has been invoked only in the derivation of the proposed theoretical model. In contrast, in the simulated scenarios a BS is in NLOS only if the direct ray connecting the standard user and the BS is blocked by one or more vehicles in the obstacle lanes.

Communications between the standard user and the serving BS are impaired only by large vehicles (namely, trucks, double-decker buses, etc.) driving on the obstacle lanes. Specifically, we consider blockages with length (τ) and width of a double-decker bus [50]. Without loss of generality, both the proposed theoretical framework and our simulations consider bi-dimensional scenarios. Although it is always possible to deploy BSs having an antenna height sufficient to prevent the vehicles in the obstacle lanes to behave as blockages, it is not always feasible in practice. For instance, in a 4-lane road section ($N_o = 2$) with $w = 3.7\,\mathrm{m}$ where the standard user drives in the middle of the lower-most user lane and the user antenna height is $1.5\,\mathrm{m}$, the BS antenna height should be greater than $12.5\,\mathrm{m}$ to allow a blockage-free scenario, which is at least twice as much the antenna height in a typical LTE-A urban deployment [51]. Therefore, we assume that the BS antenna height is $5\,\mathrm{m}$, which means that vehicles in the obstacle lanes always behave as blockages. For this reason, we do not further consider the height of the vehicles in our study.

All the remaining simulation parameters are summarized in Table V. Both our simulator and the implementation of the proposed theoretical framework are available online[4] [52].

B. Theoretical Model Assessment

In order to numerically study our mmWave highway network and assess the accuracy of our theoretical model, we first consider a road section with a length $2R = 100\,\mathrm{km}$, which ensures a simulation accuracy error of at least $10^{-7.2}$.

Considering the density λ_{BS} of process Φ_{BS}, we ideally project the BSs onto the x-axis and we define their projected mean Inter-Site-Distance (x-ISD) as $1/\lambda_{\mathrm{BS}}$.

Fig. 3 shows the probability of the standard user connecting to a LOS BS as a function of λ_{BS} for one and two obstacle

[4]The whole software package will be made publicly available at the moment of the publication of this manuscript.

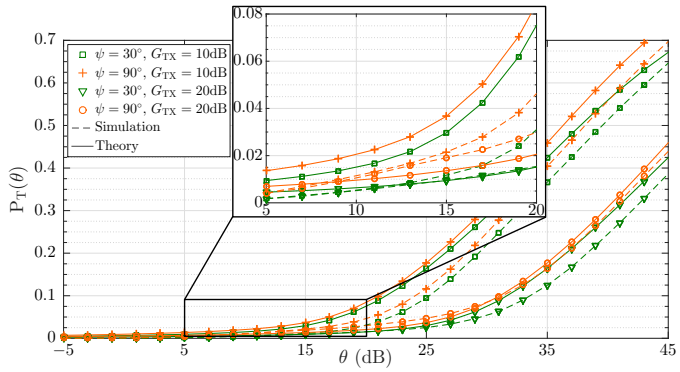

(a) $\lambda_{\mathrm{BS}} = 10^{-2}$, x-ISD = 100 m

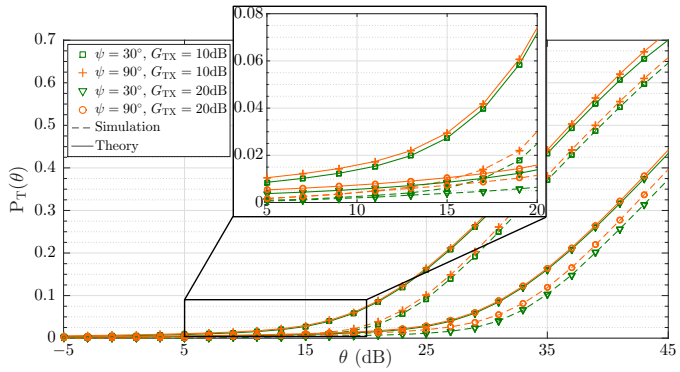

(b) $\lambda_{\mathrm{BS}} = 4 \cdot 10^{-3}$, x-ISD = 250 m

Fig. 4. SINR outage probability $\mathrm{P_T}$ as a function of the threshold θ, for $N_o = 1$, $\psi = \{30°, 90°\}$ and $G_{\mathrm{TX}} = \{10\,\mathrm{dB}, 20\,\mathrm{dB}\}$.

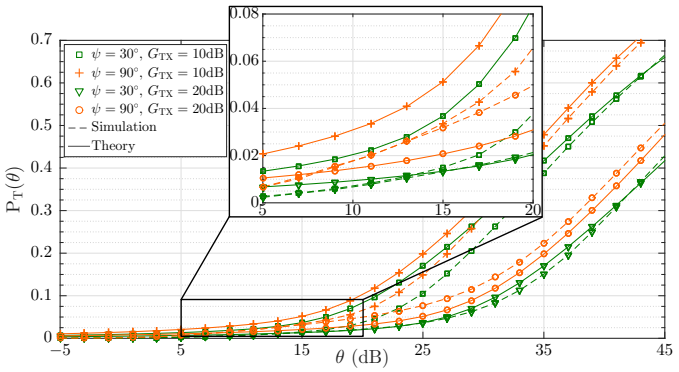

(a) $\lambda_{\mathrm{BS}} = 10^{-2}$, x-ISD = 100 m

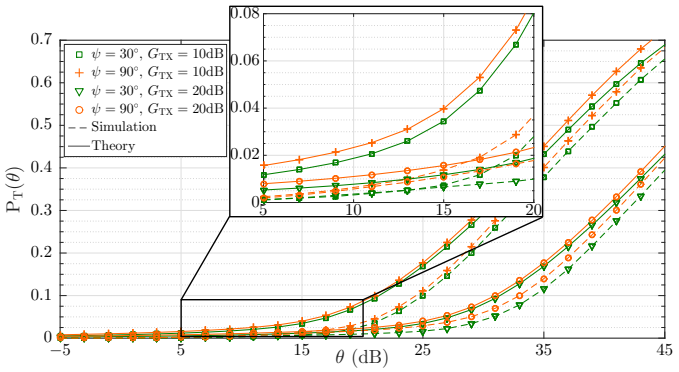

(b) $\lambda_{\mathrm{BS}} = 4 \cdot 10^{-3}$, x-ISD = 250 m

Fig. 5. SINR outage probability $\mathrm{P_T}$ as a function of the threshold θ, for $N_o = 2$, $\psi = \{30°, 90°\}$ and $G_{\mathrm{TX}} = \{10\,\mathrm{dB}, 20\,\mathrm{dB}\}$.

lanes on each side of the road. The equivalent x-ISD spans between 5 km ($\lambda_{\mathrm{BS}} = 2 \cdot 10^{-4}$) and 50 m ($\lambda_{\mathrm{BS}} = 2 \cdot 10^{-2}$). In particular, as typically happens, we observe that $\mathrm{P_L}$ is significantly greater than $\mathrm{P_N}$. Specifically, if $N_o = 1$ then, for $\lambda_{\mathrm{BS}} = 4 \cdot 10^{-3}$, the simulated value of $\mathrm{P_L}$ is equal to 0.92. When N_o increases to 2, the simulated value of $\mathrm{P_L}$ reduces to 0.90, for $\lambda_{\mathrm{BS}} = 4 \cdot 10^{-3}$.

Fig. 3 also compares our approximated theoretical expression of $\mathrm{P_L}$, as in (8), with the simulated one. We note that (8) overestimates $\mathrm{P_L}$, and, hence, (7) underestimates $\mathrm{P_N}$. However, we observe that: (i) for $\lambda_{\mathrm{BS}} \in [2 \cdot 10^{-4}, 10^{-2}]$, the overestimation error is smaller than 0.04), and (ii) for dense scenarios ($\lambda_{\mathrm{BS}} > 10^{-2}$), it never exceeds 0.02. Generally, we observe that the proposed theoretical model follows the trend of the simulated values. From Fig. 3, we also conclude that $\mathrm{P_L}$ may have a non-trivial minimum. In our scenarios, this is particularly evident when $N_o = 2$.

Remark 5.1: As we move from sparse to dense scenarios, it becomes more likely for a NLOS BS to be closer to the standard user; thus $\mathrm{P_L}$ decreases. However, this reasoning holds up to a certain value of density. In fact, at some point, the BS density becomes so high that it becomes increasingly unlikely not to have a LOS BS that is close enough to serve the standard user. This phenomenon may determine a non-trivial minimum in $\mathrm{P_L}$.

Fig. 4 shows the effect of the SINR threshold θ on the outage probability $\mathrm{P_T}(\theta)$, for $N_o = 1$, several antenna beamwidth ψ and a range of BS transmit antenna gains G_{TX}. Here, the vehicular receive antenna gain is set to $G_{\mathrm{RX}} = 10\,\mathrm{dB}$. In Fig. 4a, the x-ISD is fixed at 100 m. It should be noted that the proposed theoretical model, as in Theorem 4.2, not only follows the trend of the simulated values of $\mathrm{P_T}(\theta)$ but also it is a tight upper-bound for our simulations for the majority of the values of θ. In addition, the deviation between theory and simulation is negligible when $\theta \in [-5\,\mathrm{dB}, 15\,\mathrm{dB}]$ or $\theta \in [-5\,\mathrm{dB}, 10\,\mathrm{dB}]$, for $G_{\mathrm{TX}} = 10\,\mathrm{dB}$ or $G_{\mathrm{TX}} = 20\,\mathrm{dB}$, respectively. On the other hand, that deviation gradually increases as θ becomes larger. Nevertheless, the maximum Mean Squared Error (MSE) between simulation and theory is smaller than $1.7 \cdot 10^{-3}$. Overall, we observe the following facts:

- Changing the beamwidth from 30° to 90° alters the SINR outage probability only by a maximum of $5 \cdot 10^{-2}$. This can be intuitively explained by noting that the serving BS is likely to be close to the vertical symmetry axis of our system model. From Assumption 3.7, the standard user aligns its beam towards the serving BS. As such, the values of J and K (see Theorem 4.1) do not largely change on passing from $\psi = 30°$ to $\psi = 90°$. Thus, for the interference component to become substantial, the value of ψ should be quite large.
- Overall, we observe that when the beamwidth increases, so does $\mathrm{P_T}$. Intuitively, that is because the standard user is likely to receive a large interference contribution via the main antenna lobe.
- Increasing the value of the maximum transmit antenna gain (from 10 dB to 20 dB) results in a reduction of the

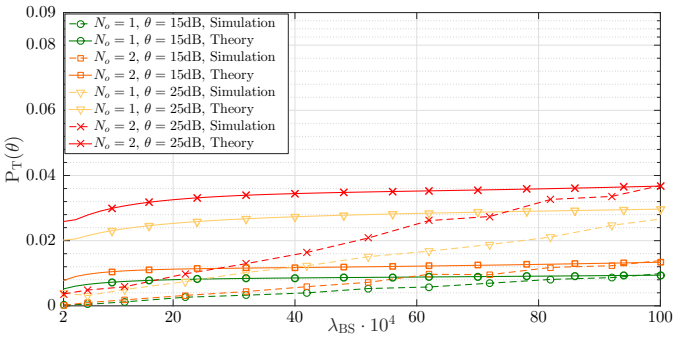

Fig. 6. SINR outage probability $\mathrm{P_T}$ as a function of the BS density λ_{BS}, for $\theta = \{15\,\mathrm{dB}, 25\,\mathrm{dB}\}$ dB, $N_o = \{1, 2\}$, $\psi = 30°$ and $G_{\mathrm{TX}} = 20\,\mathrm{dB}$.

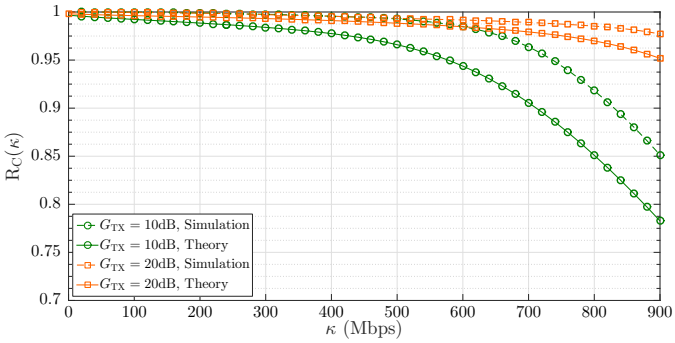

Fig. 7. Rate coverage probability $\mathrm{R_C}$ as a function of the threshold κ, for $\psi = 30°$, $G_{\mathrm{TX}} = \{10\,\mathrm{dB}, 20\,\mathrm{dB}\}$, $\lambda_{\mathrm{BS}} = 4 \cdot 10^{-3}$ and $N_o = 2$.

SINR outage probability that, for large values of θ, can be greater than 0.26. This clearly suggests that the increment on the interfering power is always smaller than or equal to the correspondent increment on the signal power. This is mainly because of the directivity of the considered antenna model and the disposition of the BSs.

Fig. 4b refers to the same scenarios as in Fig. 4a except for the x-ISD that is equal to $250\,\mathrm{m}$. In general, we observe that the comments to Fig. 4a still hold. Furthermore, the impact of the value of ψ on $\mathrm{P_T}$ becomes negligible. Intuitively, this can be explained by noting that the number of interfering BSs that are going to be received by the standard user at the maximum antenna gain decreases as λ_{BS} decreases. However, as the BS density decreases (the BSs are more sparsely deployed), it becomes more likely (up a certain extent) that the number of interfering BSs remains the same, even for a beamwidth equal to $90°$.

Fig. 5 refers to the same scenarios as Fig. 4 with two obstacle lanes on each side of the road ($N_o = 2$). In addition to the discussion for Fig. 4, we note the following:

- For the smallest value of the antenna transmit gain ($G_{\mathrm{TX}} = 10\,\mathrm{dB}$), both the simulated and the proposed theoretical model produce values of $\mathrm{P_T}$ that are negligibly greater that those when $N_o = 1$.
- For x-ISD = $100\,\mathrm{m}$ and $G_{\mathrm{TX}} = 20\,\mathrm{dB}$, the SINR outage is slightly greater that the correspondent case as in Fig. 4a. In particular, for $\theta \geq 25\,\mathrm{dB}$, we observe an increment in the simulated values of $\mathrm{P_T}$ of more than $2 \cdot 10^{-2}$.
- As soon as we refer to a sparser network scenario, x-ISD = $250\,\mathrm{m}$, the conclusions drawn for Fig. 4b also apply for Fig. 5b. Hence, the impact of ψ on $\mathrm{P_T}$ vanishes.

From Fig. 4 and Fig. 5, we already observed that the proposed theoretical model, as in Theorem 4.2, follows well the trend of the corresponding simulated values, and it is characterized by an error that is negligible for the most important values of θ (e.g., $\theta \leq 25\,\mathrm{dB}$). These facts are further confirmed by Fig. 6, which shows the value of $\mathrm{P_T}$ as as a function of λ_{BS}, for $\theta = 15\,\mathrm{dB}$ or $25\,\mathrm{dB}$, and $\psi = 30°$. In particular, as also shown in Fig. 4 and Fig. 5, as θ increases the deviation between the simulations and the theoretical model increases. However, the MSE between theory and simulation never exceeds $2.1 \cdot 10^{-3}$ in Figs. 5a and 5b. Most importantly,

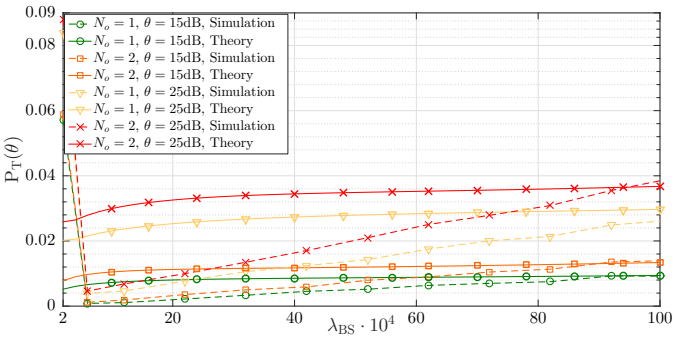

Fig. 8. SINR outage probability $\mathrm{P_T}$ as a function of the BS density λ_{BS}, for $\theta = \{15\,\mathrm{dB}, 25\,\mathrm{dB}\}$ dB, $N_o = \{1, 2\}$, $\psi = 30°$ and $G_{\mathrm{TX}} = 20\,\mathrm{dB}$. Simulation results obtained for $2R = 20\,\mathrm{km}$.

Fig. 6 further reinforces what was already observed in Fig. 4 and Fig. 5:

- As expected, $\mathrm{P_T}$ increases as N_o increases. However, when N_o passes from 1 to 2, $\mathrm{P_T}$ increases no more than $1 \cdot 10^{-2}$. Hence, we conclude that the network is particularly resilient to the number of obstacle lanes.
- The impact of λ_{BS} on the value of $\mathrm{P_T}$ is reasonably small, if compared to what happens in a typical bi-dimensional mmWave cellular network [21]. This can be justified by the same reasoning provided for Fig. 4a.

Let us consider again Fig. 6; it shows that $\mathrm{P_T}$ has only trivial minima for the considered values of θ. Specifically, for $\theta = 15\,\mathrm{dB}$ and $\theta = 25\,\mathrm{dB}$, if we refer only to the minimization of the SINR outage probability, the optimal value of λ_{BS} simply is $2 \cdot 10^{-4}$.

Fig. 7 shows the rate coverage probability as a function of the rate threshold κ, for $\psi = 30°$, $\lambda_{\mathrm{BS}} = 4 \cdot 10^{-3}$ and $N_o = 2$. From (24), we remark that the expression of $\mathrm{R_C}$ directly follows from $\mathrm{P_T}$. For this reason, we observe that the greater the gain $\mathrm{G_{TX}}$, the higher the value of $\mathrm{R_C}$. Similarly, given the network resiliency to the increment of the number of obstacle lanes, the impact of N_o on the values of $\mathrm{R_C}$ is negligible. Finally, we observe that the MSE between simulations and the proposed theoretical approximation is smaller than $1.5 \cdot 10^{-3}$.

For completeness, our model was validated by considering a significantly shorter highway section, namely $2R = 20\,\mathrm{km}$. In particular, Fig. 8 compares simulation and theoretical results for the same transmission parameters and road layout as in

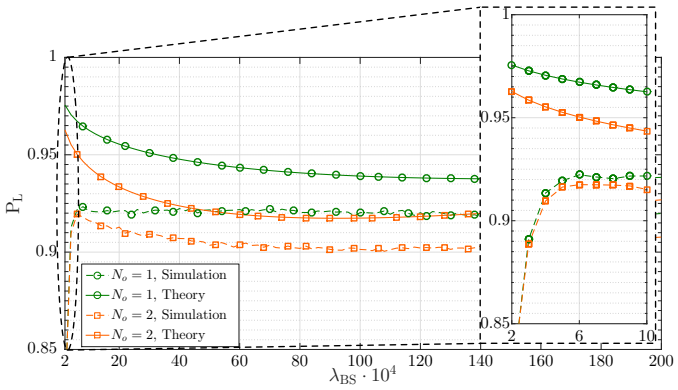

Fig. 9. Probability $\mathrm{P_L}$ that the standard users connects to a LOS BS as a function of λ_{BS}, for $N_o = 2$. Simulation results obtained for $2R = 20\,\mathrm{km}$.

Fig. 6. We observe that for $\lambda_{\mathrm{BS}} \geq 6 \cdot 10^{-4}$ simulation results are almost identical to those reported in Fig. 6, however there is a substantial deviation for $\lambda_{\mathrm{BS}} < 6 \cdot 10^{-4}$.

The aforementioned alteration can be easily explained by considering Fig. 9, which shows $\mathrm{P_L}$ as a function of λ_{BS} in the same simulated scenario as Fig. 8 (for $N_o = 2$). Also, in this case, we observe that the simulation results overlap those as in Fig. 3 for $\lambda_{\mathrm{BS}} \geq 6 \cdot 10^{-4}$. However, that does not apply for $\lambda_{\mathrm{BS}} < 6 \cdot 10^{-4}$, which has a direct impact on the results in Fig. 8. In particular, $\mathrm{P_L}$ appears to sharply decrease for very low BS densities, which is a clear side effect of considering short road sections. In fact, due to the small value of R, the simulated process regulating the position of BSs can no longer be regarded as good approximations of a PPP, for $\lambda_{\mathrm{BS}} < 6 \cdot 10^{-4}$. Despite this, we conclude that both Figs. 8 and 9 shows that the proposed theoretical model remains valid for $\lambda_{\mathrm{BS}} \geq 6 \cdot 10^{-4}$ for shorter road sections and in the case the standard user is located in the middle of a user lane.

VI. Conclusions and Future Developments

This paper has addressed the issue of characterizing the downlink performance of a mmWave network deployed along a highway section. In particular, we proposed a novel theoretical framework for characterizing the SINR outage probability and rate coverage probability of a user surrounded by large vehicles sharing the other highway lanes. Our model treated large vehicles as blockages, and hence they impact on the developed LOS/NLOS model. One of the prominent features of our system model is that BSs are systematically placed at the side of the road, and large vehicles are assumed to drive along parallel lanes. Hence, unlike a typical stochastic geometry system, we assumed that both BS and blockage positions are governed by multiple independent mono-dimensional PPPs that are not independent of translations and rotations. This modelling choice allowed the proposed theoretical framework to model different road layouts.

We compared the proposed theoretical framework with simulation results, for a number of scenarios. In particular, we observed that the proposed theoretical framework can efficiently describe the network performance, in terms of SINR outage and rate coverage probability. Furthermore, we observed the following fundamental properties:

- Reducing the antenna beamwidth from 90° to 30° does not necessarily have a disruptive impact on the SINR outage probability, and hence, on the rate coverage probability.
- In contrast with bi-dimensional mmWave cellular networks, the BS density does not immediatly affect the network performance.
- Overall, for a fixed SINR threshold, the SINR outage probability is minimized by low BS densities, corresponding to sparse network deployments.

In the future, we plan to extend the proposed model by making it able to characterize mmWave vehicular communications in urban and suburban environments with irregular road layouts.

Appendix A
Proof of Theorem 4.1

For $\mathbb{E}_1 = \{\mathrm{L}, \mathrm{N}\}$, the Laplace transform of $\mathrm{I_{S,E}}$ can be expressed as:

$$\mathcal{L}_{\mathrm{I_{S,E}},\mathbb{E}_1}(s) = \mathbb{E}_{\Phi_{\mathrm{S,E}}}\left(\prod_{j\in\Phi_{\mathrm{S,E}}} \mathbb{E}_h \mathbb{E}_\Delta\left(e^{-s|h_j|^2\Delta_j \ell(r_j)}\right)\right) \quad (25)$$

$$\overset{(i)}{=} \exp\left(-\mathbb{E}_\Delta \mathbb{E}_h \int_{w(N_o+1)}^{+\infty} e^{-sh\Delta r^{-\alpha_{\mathrm{E}}}} \cdot \frac{2rq\lambda_{\mathrm{E}}}{\sqrt{r^2 - w^2(N_o+1)^2}}\, dr\right) \quad (26)$$

where $\mathbb{E}_{\Phi_{\mathrm{S,E}}}$ represents the expectation with respect to the distance of each BS in $\Phi_{\mathrm{S,E}}$ from O. Similarly, operators $\mathbb{E}_\Delta$ and $\mathbb{E}_h$ signify the expectation with respect to the overall antenna gain and the small-scale fading gain associated with the transmissions of each BS, respectively. We observe that equality (i) arises from the definition of a probability generating functional (pgfl) of a PPP [41, Definition 4.3] and the mapping theorem applied to $\Phi_{\mathrm{S,E}}$ [41, Theorem 2.34]. In addition, the pgfl allows us to drop the relation to a specific BS j in the terms expressing a distance of a BS to O, its channel and antenna gains. For this reason, in the integrand function, we simply refer to terms r, h and Δ.

Let a and b be two real numbers greater than or equal to $w(N_o+1)$ and such that $a \leq b$. With regards to (26), we condition with respect to a specific value of h and Δ, and we approximate the following term[5]:

$$\int_a^b e^{-sh\Delta r^{-\alpha_{\mathrm{E}}}} \frac{2rq\lambda_{\mathrm{E}}}{\sqrt{r^2 - w^2(N_o+1)^2}}\, dr$$
$$\overset{(i)}{=} \int_{\sqrt{a^2-w^2(N_o+1)^2}}^{\sqrt{b^2-w^2(N_o+1)^2}} e^{-sh\Delta(t^2+w^2(N_o+1)^2)^{-\alpha_{\mathrm{E}}/2}} 2q\lambda_{\mathrm{E}}\, dt$$

[5]For clarity, we define $[f(x)]_{x=a}^b = f(b) - f(a)$.

$$\overset{(ii)}{\cong} \int_a^b e^{-sh\Delta t^{-\alpha_{\mathrm{E}}}} 2q\lambda_{\mathrm{E}}\, dt \tag{27}$$

$$\overset{(iii)}{=} \underbrace{-2q\lambda_{\mathrm{E}} \int_{a^{-\alpha_{\mathrm{E}}}}^{b^{-\alpha_{\mathrm{E}}}} (1-e^{-sh\Delta x})\alpha_{\mathrm{E}}^{-1} x^{-\alpha_{\mathrm{E}}^{-1}-1}\, dx}_{\Theta(h,\Delta)}$$

$$\overset{(iv)}{=} \underbrace{2q\lambda_{\mathrm{E}} \left[(1-e^{-sh\Delta x})x^{-\alpha_{\mathrm{E}}^{-1}}\right]_{x=a^{-\alpha_{\mathrm{E}}}}^{b^{-\alpha_{\mathrm{E}}}}}$$

$$\underbrace{-2q\lambda_{\mathrm{E}} \int_{a^{-\alpha_{\mathrm{E}}}}^{b^{-\alpha_{\mathrm{E}}}} sh\Delta x^{-\frac{1}{\alpha_{\mathrm{E}}}} e^{-sh\Delta x}\, dx}_{\Lambda(h,\Delta)}, \tag{28}$$

where (i) arises from the change of variable $t \leftarrow \sqrt{r^2 - w^2(N_o+1)^2}$, while (ii) assumes that $w(N_o+1)$ is equal to 0 (see Section V-B for the validation of the proposed theoretical framework). Equality (iii) arises by applying the changes of variable $y \leftarrow t^{\alpha_{\mathrm{E}}}$ and then $x \leftarrow y^{-1}$. In addition, in (iv), we resort to an integration by parts.

With regards to (28), we keep the conditioning to Δ and calculate the expectation of $\Theta(h,\Delta)$ and $\Lambda(h,\Delta)$, with respect to h. From Assumption 4.1, it should be noted that we refer to a Rayleigh channel model, and, hence, the following relation holds:

$$\mathbb{E}_h\left[\Theta(h,\Delta)\right] = 2q\lambda_{\mathrm{E}} \left[x^{-\alpha_{\mathrm{E}}^{-1}} \left(1 - \frac{1}{s\Delta x+1}\right)\right]_{x=a^{-\alpha_{\mathrm{E}}}}^{b^{-\alpha_{\mathrm{E}}}}. \tag{29}$$

Term $\mathbb{E}_h\left[\Lambda(h,\Delta)\right]$ can be found as follows:

$$\begin{aligned}\mathbb{E}_h\left[\Lambda(h,\Delta)\right] &= -2q\lambda_{\mathrm{E}} \int_{a^{-\alpha_{\mathrm{E}}}}^{b^{-\alpha_{\mathrm{E}}}} x^{-\frac{1}{\alpha_{\mathrm{E}}}} \\ &\quad \cdot \int_0^{\infty} sh\Delta e^{-(s\Delta x+1)h}\, dh\, dx \\ &= -2q\lambda_{\mathrm{E}} \int_{a^{-\alpha_{\mathrm{E}}}}^{b^{-\alpha_{\mathrm{E}}}} x^{-\frac{1}{\alpha_{\mathrm{E}}}} \frac{\partial}{\partial x}\left(-\frac{1}{s\Delta x+1}\right) dx \\ &\overset{(i)}{=} -2q\lambda_{\mathrm{E}}(s\Delta)^{\frac{1}{\alpha_{\mathrm{E}}}} \int_{-(s\Delta a^{-\alpha_{\mathrm{E}}}+1)^{-1}}^{-(s\Delta b^{-\alpha_{\mathrm{E}}}+1)^{-1}} \left(-\frac{1}{t}-1\right)^{-\frac{1}{\alpha_{\mathrm{E}}}} dt\end{aligned} \tag{30}$$

$$\overset{(ii)}{=} -2q\lambda_{\mathrm{E}}(s\Delta)^{\frac{1}{\alpha_{\mathrm{E}}}} \left[t(-t^{-1})^{-\frac{1}{\alpha_{\mathrm{E}}}} \Gamma\left(\frac{1}{\alpha_{\mathrm{E}}}+1\right) \cdot {}_2\tilde{F}_1\left(\frac{1}{\alpha_{\mathrm{E}}}, \frac{1}{\alpha_{\mathrm{E}}}+1; \frac{1}{\alpha_{\mathrm{E}}}+2; -t\right)\right]_{t=-(s\Delta a^{-\alpha_{\mathrm{E}}}+1)^{-1}}^{-(s\Delta b^{-\alpha_{\mathrm{E}}}+1)^{-1}},$$

where (i) arises from the change of variable $t \leftarrow -\frac{1}{s\Delta x+1}$. Let us signify with ${}_2\tilde{F}_1(a,b;c;z) = \sum_{k=0}^{\infty} \frac{\{a\}_k \{b\}_k}{\{c\}_k} \frac{z^k}{k!}$ the Gauss hypergeometric function[6]. We observe that the integral as in equality (i) is closely related to that as in [54, Eq. (3.228.3)], and after some manipulations we have equality (ii).

From the approximation in (27), it follows that $a \cong \sqrt{a^2 - w^2(N_o+1)^2}$ and $b \cong \sqrt{b^2 - w^2(N_o+1)^2}$.

[6]We observe that z is always a real number, which allows us to significantly reduce the complexity of the whole numerical integration process [53].

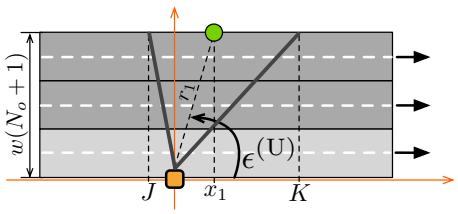

Fig. 10. Case where the standard user is served by a BS from the upper side of the road.

Hence, we observe that $\mathcal{L}_{\mathrm{I_{S,E}},\mathbb{E}_1}(s)$, conditioned on the gain Δ (see (9)), can be expressed as follows:

$$\begin{aligned}\mathcal{L}_{\mathrm{I_{S,E}},\mathbb{E}_1}(s) &\cong \mathcal{L}_{\mathrm{I_{S,E}},\mathbb{E}_1}(s;a,b,\Delta)\Big|_{a=0,b=+\infty} \\ &= \exp\left(-\left(\mathbb{E}_h[\Theta(h,\Delta)] + \mathbb{E}_h[\Lambda(h,\Delta)]\Big|_{a=0,b=+\infty}\right)\right).\end{aligned} \tag{31}$$

Let us focus on the transmit antenna gain of the j-th interfering BS, which has a PDF that depends on the distance r_j and the orientation of the beam ϵ_i. To take into account the exact formulation of the BS transmit antenna gain would make the performance model intractable. As such, we instead make the approximation that the transmit antenna gain is always equal to g_{TX}.

With regards to (25), we observe that after conditioning on the standard user being connected to a BS at a distance r_1 from O, then the receive antenna gain g of the interfering BSs j is determined by the parameter list $< |x_1|, p, r, \mathbb{S}_1, \mathbb{E}_1, \mathrm{S}, \mathrm{E} >$, where: (i) $|x_1|$ is the absolute value of the x-axis coordinate of BS 1, (ii) p captures the fact that the interfering BS is at a location on the positive (right-hand side of y-axis, RX) or negative side (left-hand side of y-axis, LX) of the x-axis, and (iii) r is the distance of the interfering BS to O.

Let us consider the x-axis coordinates J and K of the points where the two rays defining the antenna beam of the standard user intersect the side of the road, as shown in Fig. 10. The receive antenna gain of the interfering BS also depends on: (i) the fact the standard user connects to a BS on the upper/bottom side of the road ($\mathbb{S}_1 \in \{\mathrm{U},\mathrm{B}\}$), that can be in LOS/NLOS ($\mathbb{E}_1 \in \{\mathrm{L},\mathrm{N}\}$) with respect to the standard user, (ii) the values of S and E, and (iii) the specific configuration of the values of $|x_1|$, J and K. By invoking the same approximation as in (27), we say that $r \cong \sqrt{r^2 - w^2(N_o+1)^2}$ and the following parameters determine the receiver gain:

- $\mathbb{S}_1 = \mathrm{U}$, $\mathbb{E}_1 = \mathrm{L}$, $\mathrm{S} = \mathrm{U}$ and $\mathrm{E} = \mathrm{L}$ - we divide this case into the following subcases:
  - If the value of $|x_1|$ is such that $J > 0$ - we observe that there are no LOS BSs at a distance smaller than $|x_1|$. Hence, it follows that

$$g = G_{\mathrm{RX}} \quad \text{if} \quad \begin{cases}|x_1| \le r \le K \\ p = \mathrm{RX}\end{cases} \tag{32}$$

$$g = g_{\mathrm{RX}} \quad \text{if} \quad \begin{cases}K \le r \le +\infty \\ p = \mathrm{RX}\end{cases} \text{ or } \begin{cases}|x_1| \le r \le +\infty \\ p = \mathrm{LX}\end{cases} \tag{33}$$

  - If $J \le 0$ - by following the same reasoning as before, in addition to the case as in (32), it follows that

$$g = g_{\mathrm{RX}} \quad \text{if} \quad \begin{cases}K \le r \le +\infty \\ p = \mathrm{RX}\end{cases} \text{ or } \begin{cases}|J| \le r \le +\infty \\ p = \mathrm{LX}\end{cases} \tag{34}$$

$$g = G_{\mathrm{RX}} \quad \text{if} \quad \begin{cases} |x_1| \leq r \leq |J| \\ p = \mathrm{LX} \end{cases} \tag{35}$$

- $\mathbb{S}_1 = \mathrm{U}$, $\mathbb{E}_1 = \mathrm{L}$, $\mathrm{S} = \mathrm{U}$ and $\mathrm{E} = \mathrm{N}$ - we apply the same reasoning as before by bearing in mind that it is impossible for a NLOS BS to be at a distance that is smaller than $\mathrm{A_N}(r_1)$ to O. Equivalently, it is impossible for a NLOS BS to be associated with a x-axis coordinate smaller than $x_{\mathrm{N}}(r_1) = \sqrt{(\mathrm{A_N}(r_1))^2 - w^2(N_o+1)^2}$. In particular, for $J \leq 0$, the value of g can be derived as in (32) and (34)-(35), where term $|x_1|$ is replaced by $x_{\mathrm{N}}(r_1)$. On the other hand, for $J > 0$, the value of g can be expressed as follows:

$$g = g_{\mathrm{RX}} \quad \text{if} \quad \begin{cases} x_{\mathrm{N}}(r_1) \leq r \leq J \text{ or } K \leq r \leq +\infty \\ p = \mathrm{RX} \end{cases} \quad \text{or} \quad \begin{cases} x_{\mathrm{N}}(r_1) \leq r \leq +\infty \\ p = \mathrm{LX} \end{cases} \tag{36}$$

$$g = G_{\mathrm{RX}} \quad \text{if} \quad \begin{cases} J \leq r \leq K \\ p = \mathrm{RX} \end{cases} \tag{37}$$

- $\mathbb{S}_1 = \mathrm{U}$, $\mathbb{E}_1 = \mathrm{L}$, $\mathrm{S} = \mathrm{B}$ and $\mathrm{E} = \mathrm{L}$ - from Assumption 3.7, we observe that g is always equal to g_{RX}. In addition, we note that it is not possible to have a LOS BS at a distance smaller than r_1. Hence, we have only two possible configurations:

$$g = g_{\mathrm{RX}} \quad \text{if} \quad \begin{cases} |x_1| \leq r \leq +\infty \\ p = \mathrm{RX} \end{cases} \text{ or } \begin{cases} |x_1| \leq r \leq +\infty \\ p = \mathrm{LX} \end{cases} \tag{38}$$

- $\mathbb{S}_1 = \mathrm{U}$, $\mathbb{E}_1 = \mathrm{L}$, $\mathrm{S} = \mathrm{B}$ and $\mathrm{E} = \mathrm{N}$ - similarly to the previous case, we observe that g is equal to g_{RX} and it is not possible to have a NLOS BS at a distance smaller than $x_{\mathrm{N}}(r_1)$. Hence, we have the following cases:

$$g = g_{\mathrm{RX}} \quad \text{if} \quad \begin{cases} x_{\mathrm{N}}(r_1) \leq r \leq +\infty \\ p = \mathrm{RX} \end{cases} \text{ or } \begin{cases} x_{\mathrm{N}}(r_1) \leq r \leq +\infty \\ p = \mathrm{LX} \end{cases} \tag{39}$$

- With regards the remaining parameter combinations where $\mathbb{S}_1 = \mathrm{U}$, $\mathbb{E}_1 = \mathrm{N}$, we observe the following cases:
  - $\mathrm{S} = \mathrm{U}$, $\mathrm{E} = \mathrm{L}$ - we define $x_{\mathrm{L}}(r_1) = \sqrt{(\mathrm{A_L}(r_1))^2 - w^2(N_o+1)^2}$. If $x_{\mathrm{L}}(r_1) > K$, refer to (38) and replace $|x_1|$ with $x_{\mathrm{L}}(r_1)$. Otherwise, refer to (32)-(35) and replace $|x_1|$ with $x_{\mathrm{L}}(r_1)$.
  - $\mathrm{S} = \mathrm{U}$, $\mathrm{E} = \mathrm{N}$ - refer to (32)-(35).
  - $\mathrm{S} = \mathrm{B}$, $\mathrm{E} = \mathrm{L}$ - refer to (38) and replace $|x_1|$ with $x_{\mathrm{L}}(r_1)$.
  - $\mathrm{S} = \mathrm{B}$, $\mathrm{E} = \mathrm{N}$ - refer to (38).
- By following the above approach, it is possible to derive all the remaining configurations. In particular, the characterization of g, for a parameter configuration where $\mathbb{S}_1 = \mathrm{B}$ and $\mathrm{S} = \mathrm{B}$ ($\mathbb{S}_1 = \mathrm{B}$ and $\mathrm{S} = \mathrm{U}$) follows exactly the same rule of the corespondent parameter list, where $\mathbb{S}_1 = \mathrm{U}$ and $\mathrm{S} = \mathrm{U}$ ($\mathbb{S}_1 = \mathrm{U}$ and $\mathrm{S} = \mathrm{B}$).

The aforementioned parameter configurations are also summarized in Table IV. With regards to parameter p, we observe that the probability $\mathbb{P}[p]$ of p being equal to DX or RX is 0.5.

Consider (31), all the elements are in place to explicitly calculate the expectation with respect to Δ. In particular, it follows that $\mathcal{L}_{\mathrm{I_{S,E}}}(s)$ can be expressed as:

$$\begin{aligned}
\mathcal{L}_{\mathrm{I_{S,E,\mathbb{E}_1}}}(s) &\overset{(i)}{\cong} \exp\left(-\mathbb{E}_\Delta\left(\mathbb{E}_h[\Theta(h,\Delta)+\Lambda(h,\Delta)]\Big|_{a=0,b=+\infty}\right)\right) \\
&\overset{(ii)}{\cong} \exp\left(-\sum_{\substack{\mathbb{S}_1\in\{\mathrm{U,B}\} \\ (a,b,\Delta)\in\mathcal{C}_{|\mathrm{x_1}|,\mathbb{S}_1,\mathbb{E}_1,\mathrm{S,E}}}} \mathbb{P}[p]\left(\mathbb{E}_h[\Theta(h,\Delta)+\Lambda(h,\Delta)]\Big|_{a,b,\Delta}\right)\right) \\
&= \prod_{\substack{\mathbb{S}_1\in\{\mathrm{U,B}\}, \\ (a,b,\Delta)\in\mathcal{C}_{|\mathrm{x_1}|,\mathbb{S}_1,\mathbb{E}_1,\mathrm{S,E}}}} \exp\left(-\frac{1}{2}\left(\mathbb{E}_h[\Theta(h,\Delta)]\Big|_{a,b,\Delta} + \mathbb{E}_h[\Lambda(h,\Delta)]\Big|_{a,b,\Delta}\right)\right) \\
&= \prod_{\substack{\mathbb{S}_1\in\{\mathrm{U,B}\}, \\ (a,b,\Delta)\in\mathcal{C}_{|\mathrm{x_1}|,\mathbb{S}_1,\mathbb{E}_1,\mathrm{S,E}}}} \sqrt{\mathcal{L}_{\mathrm{I_{S,E},\mathbb{E}_1}}(s;a,b,\Delta)},
\end{aligned} \tag{40}$$

where (i) is (31). From the previous discussion, for a given $|x_1|$, Δ can either be equal to $g_{\mathrm{TX}}g_{\mathrm{RX}}$ or $g_{\mathrm{TX}}G_{\mathrm{RX}}$. In particular, the value of Δ is determined by the list of parameters $< |\mathrm{x_1}|, \mathbb{S}_1, \mathbb{E}_1, \mathrm{S}, \mathrm{E} >$, where terms a and b are the minimum and maximum distance r to an interfering BS, respectively. We define sequence $\mathcal{C}_{|\mathrm{x_1}|,\mathbb{S}_1,\mathbb{E}_1,\mathrm{S,E}}$. This sequence consists of all the possible parameter configurations (a,b,Δ). For instance, if $\mathbb{S}_1 = \mathrm{U}$, $\mathbb{E}_1 = \mathrm{L}$, $\mathrm{S} = \mathrm{U}$, $\mathrm{E} = \mathrm{L}$ and $J > 0$, sequence $\mathcal{C}_{|\mathrm{x_1}|,\mathbb{S}_1,\mathbb{E}_1,\mathrm{S,E}}$ consists of: $(|x_1|, K, g_{\mathrm{TX}}G_{\mathrm{RX}})$, $(K, +\infty, g_{\mathrm{TX}}g_{\mathrm{RX}})$ and $(|x_1|, +\infty, g_{\mathrm{TX}}g_{\mathrm{RX}})$. We note that each element of a sequence $\mathcal{C}_{|\mathrm{x_1}|,\mathbb{S}_1,\mathbb{E}_1,\mathrm{S,E}}$ occurs with probability $\mathbb{P}[p]$. Furthermore, we observe that like those in (38) and (39), sequence $\mathcal{C}_{|\mathrm{x_1}|,\mathbb{S}_1,\mathbb{E}_1,\mathrm{S,E}}$ lists twice the same parameter configuration. Given these reasons, the term $\mathbb{E}_\Delta(\mathbb{E}_h[\Theta(h,\Delta)+\Lambda(h,\Delta)]\big|_{a=0,b=+\infty})$ can be approximated as in (ii). After some manipulations of (ii), we get to (11), which concludes the proof.

REFERENCES

[1] D. Evans, "The Internet of Things," Cisco IBSG, Tech. Rep., Apr. 2011. [Online]. Available: https://www.cisco.com/c/dam/en_us/about/ac79/docs/innov/IoT_IBSG_0411FINAL.pdf

[2] "Preliminary Statement of Policy Concerning Automated Vehicles," U.S. Department of Transportation, National Highway Traffic Safety Administration (NHTSA), Tech. Rep., 2013. [Online]. Available: http://www.nhtsa.gov/staticfiles/rulemaking/pdf/Automated_Vehicles_Policy.pdf

[3] "C-ITS Platform," European Commission, Tech. Rep., Jan. 2016. [Online]. Available: http://ec.europa.eu/transport/themes/its/doc/c-its-platform-final-report-january-2016.pdf

[4] "5G-PPP White Paper on Automotive Vertical Sector," 5G Infrastructure Public Private Partnership, Tech. Rep., Oct. 2015. [Online]. Available: https://5g-ppp.eu/wp-content/uploads/2014/02/5G-PPP-White-Paper-on-Automotive-Vertical-Sectors.pdf

[5] N. Lu, N. Cheng, N. Zhang, X. Shen, and J. W. Mark, "Connected Vehicles: Solutions and Challenges," *IEEE Internet Things J.*, vol. 1, no. 4, pp. 289–299, Aug. 2014.

[6] E. Uhlemann, "Connected-Vehicles Applications Are Emerging," *IEEE Veh. Technol. Mag.*, vol. 11, no. 1, pp. 25–96, Mar. 2016.

[7] J. Choi, V. Va, N. Gonzalez-Prelcic, R. Daniels, C. R. Bhat, and R. W. Heath, "Millimeter-Wave Vehicular Communication to Support Massive Automotive Sensing," *IEEE Commun. Mag.*, vol. 54, no. 12, pp. 160–167, Dec. 2016.

[8] J. G. Andrews, S. Buzzi, W. Choi, S. V. Hanly, A. Lozano, A. C. K. Soong, and J. C. Zhang, "What Will 5G Be?" *IEEE J. Sel. Areas Commun.*, vol. 32, no. 6, pp. 1065–1082, Jun. 2014.

[9] T. Nitsche, C. Cordeiro, A. B. Flores, E. W. Knightly, E. Perahia, and J. C. Widmer, "IEEE 802.11ad: Directional 60 GHz Communication For Multi-Gigabit-per-Second Wi-Fi," *IEEE Commun. Mag.*, vol. 52, no. 12, pp. 132–141, Dec. 2014.

[10] J. B. Kenney, "Dedicated Short-Range Communications (DSRC) Standards in the United States," *Proceedings of the IEEE*, vol. 99, no. 7, pp. 1162–1182, Jul. 2011.

[11] G. Karagiannis, O. Altintas, E. Ekici, G. Heijenk, B. Jarupan, K. Lin, and T. Weil, "Vehicular Networking: A Survey and Tutorial on Requirements, Architectures, Challenges, Standards and Solutions," *IEEE Commun. Surveys Tuts.*, vol. 13, no. 4, pp. 584–616, Fourth 2011.

[12] E. Uhlemann, "Introducing Connected Vehicles," *IEEE Veh. Technol. Mag.*, vol. 10, no. 1, pp. 23–31, Mar. 2015.

[13] E. G. Strom, "On Medium Access and Physical Layer Standards for Cooperative Intelligent Transport Systems in Europe," *Proceedings of the IEEE*, vol. 99, no. 7, pp. 1183–1188, Jul. 2011.

[14] M. Xie, Y. Shang, Z. Yang, Y. Jing, and H. Zhou, "A Novel MBSFN Scheme for Vehicle-to-Vehicle Safety Communication Based on LTE Network," in *Proc. of IEEE VTC-Fall 2015*, Boston, Massachusetts, USA, Sep. 2015, pp. 1–5.

[15] G. Araniti, C. Campolo, M. Condoluci, A. Iera, and A. Molinaro, "LTE for Vehicular Networking: A Survey," *IEEE Commun. Mag.*, vol. 51, no. 5, pp. 148–157, May 2013.

[16] T. Rappaport, R. Heath, R. Daniels, and J. Murdock, *Millimeter Wave Wireless Communications*, ser. Communication engineering and emerging technologies. Prentice Hall, 2014.

[17] T. S. Rappaport, F. Gutierrez, E. Ben-Dor, J. N. Murdock, Y. Qiao, and J. I. Tamir, "Broadband Millimeter-Wave Propagation Measurements and Models Using Adaptive-Beam Antennas for Outdoor Urban Cellular Communications," *IEEE Trans. Antennas Propag.*, vol. 61, no. 4, pp. 1850–1859, Apr. 2013.

[18] H. Shokri-Ghadikolaei, C. Fischione, G. Fodor, P. Popovski, and M. Zorzi, "Millimeter Wave Cellular Networks: A MAC Layer Perspective," *IEEE Trans. Commun.*, vol. 63, no. 10, pp. 3437–3458, Oct. 2015.

[19] "Leading train operators granted innovation funding," RSSB, Tech. Rep., Jul. 2015. [Online]. Available: https://www.rssb.co.uk/Library/about-rssb/2015-07-press-release-leading-train-operators-granted-innovation-funding.pdf

[20] J. Gozalves, "Fifth-Generation Technologies Trials," *IEEE Veh. Technol. Mag.*, vol. 11, no. 2, pp. 5–13, Jun. 2016.

[21] T. Bai and R. W. Heath Jr., "Coverage and Rate Analysis for Millimeter-Wave Cellular Networks," *IEEE Trans. Wireless Commun.*, vol. 14, no. 2, pp. 1100–1114, Feb. 2015.

[22] T. S. Rappaport, S. Sun, R. Mayzus, H. Zhao, Y. Azar, K. Wang, G. N. Wong, J. K. Schulz, M. Samimi, and F. Gutierrez, "Millimeter Wave Mobile Communications for 5G Cellular: It Will Work!" *IEEE Access*, vol. 1, pp. 335–349, 2013.

[23] S. Hasan, N. Siddique, and S. Chakraborty, *Intelligent Transport Systems: 802.11-based Roadside-to-Vehicle Communications*. Springer New York, 2012.

[24] C. Lochert, B. Scheuermann, C. Wewetzer, A. Luebke, and M. Mauve, "Data Aggregation and Roadside Unit Placement for a VANET Traffic Information System," in *Proc. of the fifth ACM international workshop on VehiculAr Inter-NETworking*, San Francisco, California, USA, 2008, pp. 58–65.

[25] O. Trullols, M. Fiore, C. Casetti, C. Chiasserini, and J. B. Ordinas, "Planning roadside infrastructure for information dissemination in intelligent transportation systems," *ELSEVIER Computer Communications*, vol. 33, no. 4, pp. 432 – 442, 2010.

[26] A. Ghosh, T. A. Thomas, M. C. Cudak, R. Ratasuk, P. Moorut, F. W. Vook, T. S. Rappaport, G. R. MacCartney, S. Sun, and S. Nie, "Millimeter-Wave Enhanced Local Area Systems: A High-Data-Rate Approach for Future Wireless Networks," *IEEE J. Sel. Areas Commun.*, vol. 32, no. 6, pp. 1152–1163, Jun. 2014.

[27] G. Zhang, T. Q. S. Quek, M. Kountouris, A. Huang, and H. Shan, "Fundamentals of Heterogeneous Backhaul Design - Analysis and Optimization," *IEEE Trans. Commun.*, vol. 64, no. 2, pp. 876–889, Feb. 2016.

[28] S. Singh, M. N. Kulkarni, A. Ghosh, and J. G. Andrews, "Tractable Model for Rate in Self-Backhauled Millimeter Wave Cellular Networks," *IEEE J. Sel. Areas Commun.*, vol. 33, no. 10, pp. 2196–2211, Oct. 2015.

[29] D. Maamari, N. Devroye, and D. Tuninetti, "Coverage in mmWave Cellular Networks With Base Station Co-Operation," *IEEE Trans. Wireless Commun.*, vol. 15, no. 4, pp. 2981–2994, Apr. 2016.

[30] R. Baldemair, T. Irnich, K. Balachandran, E. Dahlman, G. Mildh, Y. Selén, S. Parkvall, M. Meyer, and A. Osseiran, "Ultra-Dense Networks in Millimeter-Wave Frequencies," *IEEE Commun. Mag.*, vol. 53, no. 1, pp. 202–208, Jan. 2015.

[31] M. D. Renzo, "Stochastic Geometry Modeling and Analysis of Multi-Tier Millimeter Wave Cellular Networks," *IEEE Trans. Wireless Commun.*, vol. 14, no. 9, pp. 5038–5057, Sep. 2015.

[32] A. B. Reis, S. Sargento, F. Neves, and O. Tonguz, "Deploying Roadside Units in Sparse Vehicular Networks: What Really Works and What Does Not," *IEEE Trans. Veh. Technol.*, vol. 63, no. 6, pp. 2794–2806, Jul. 2014.

[33] K. Rostamzadeh and S. Gopalakrishnan, "Analysis of Message Delivery Delay in Vehicular Networks," *IEEE Trans. Veh. Technol.*, vol. 64, no. 10, pp. 4770–4779, Oct. 2015.

[34] N. Akhtar, S. C. Ergen, and O. Ozkasap, "Vehicle Mobility and Communication Channel Models for Realistic and Efficient Highway VANET Simulation," *IEEE Trans. Veh. Technol.*, vol. 64, no. 1, pp. 248–262, Jan. 2015.

[35] M. J. Farooq, H. ElSawy, and M. S. Alouini, "A Stochastic Geometry Model for Multi-Hop Highway Vehicular Communication," *IEEE Trans. Wireless Commun.*, vol. 15, no. 3, pp. 2276–2291, Mar. 2016.

[36] M. Haenggi, J. G. Andrews, F. Baccelli, O. Dousse, and M. Franceschetti, "Stochastic Geometry and Random Graphs for the Analysis and Design of Wireless Networks," *IEEE J. Sel. Areas Commun.*, vol. 27, no. 7, pp. 1029–1046, Sep. 2009.

[37] S. P. Weber, X. Yang, J. G. Andrews, and G. de Veciana, "Transmission Capacity of Wireless Ad-Hoc Networks with Outage Constraints," *IEEE Trans. Inf. Theory*, vol. 51, no. 12, pp. 4091–4102, Dec. 2005.

[38] C.-H. Lee, C.-Y. Shih, and Y.-S. Chen, "Stochastic Geometry Based Models for Modeling Cellular Networks in Urban," *Springer Wireless Networks*, vol. 19, no. 6, pp. 1063–1072, 2013.

[39] H. ElSawy, E. Hossain, and M. Haenggi, "Stochastic Geometry for Modeling, Analysis, and Design of Multi-Tier and Cognitive Cellular Wireless Networks: A Survey," *IEEE Commun. Surveys Tuts.*, vol. 15, no. 3, pp. 996–1019, Third 2013.

[40] S. Singh, H. S. Dhillon, and J. G. Andrews, "Offloading in Heterogeneous Networks: Modeling, Analysis, and Design Insights," *IEEE Trans. Wireless Commun.*, vol. 12, no. 5, pp. 2484–2497, May 2013.

[41] M. Haenggi, *Stochastic Geometry for Wireless Networks*, ser. Stochastic Geometry for Wireless Networks. Cambridge University Press, 2013.

[42] "ns3-mmwave." [Online]. Available: https://github.com/nyuwireless/ns3-mmwave

[43] Z. Pi and F. Khan, "An introduction to millimeter-wave mobile broadband systems," *IEEE Commun. Mag.*, vol. 49, no. 6, pp. 101–107, Jun. 2011.

[44] M. Haenggi and R. K. Ganti, "Interference in Large Wireless Networks," *Foundations and Trends in Networking, Now Publishers*, vol. 3, no. 2, pp. 127–248, 2008.

[45] S. Weber and M. Kam, "Computational Complexity of Outage Probability Simulations in Mobile Ad-Hoc Networks," in *Proc. of the 39th Annual Conference on Information Sciences and Systems (CISS)*, Baltimore, Maryland, USA, Mar. 2005.

[46] V. Kanagaraj, G. Asaithambi, C. N. Kumar, K. K. Srinivasan, and R. Sivanandan, "Evaluation of Different Vehicle Following Models Under Mixed Traffic Conditions," *Procedia - Social and Behavioral Sciences*, vol. 104, pp. 390–401, 2013.

[47] C. Bettstetter, "Mobility Modeling in Wireless Networks: Categorization, Smooth Movement, and Border Effects," *SIGMOBILE Mob. Comput. Commun. Rev.*, vol. 5, no. 3, pp. 55–66, Jul. 2001.

[48] P. Ioannou, *Automated Highway Systems*. Springer US, 2013.

[49] D. Fambro, K. Fitzpatrick, and R. Koppa, *Determination of Stopping Sight Distances*, ser. Determination of stopping sight distances. National Academy Press, 1997.

[50] "Routemaster Spec Sheet," Wrightbus, Tech. Rep., 2014. [Online]. Available: http://www.wrightsgroup.com/datasheets/Routemaster\%20spec\%20sheet.pdf

[51] "3GPP TR 36.873," 3GPP, Tech. Rep., 2013.

[52] "Proposed simulation framework and theoretical model." [Online]. Available: https://www.dropbox.com/s/r6wiuu01k0r0kt3/src.tar.bz2

[53] R. K. S. Hankin, "Numerical evaluation of the Gauss hypergeometric function with the hypergeo package," *The R Journal*, vol. 7, no. 2, pp. 81–88, Dec. 2015.

[54] A. Jeffrey and D. Zwillinger, *Table of Integrals, Series, and Products*, ser. Table of Integrals, Series, and Products Series. Elsevier Science, 2007.